Neuron

Article

Dissociating distinct cortical networks associated with subregions of the human medial temporal lobe using precision neuroimaging

Highlights

- Group-level imaging blurs fine anatomical details in the medial temporal lobe (MTL)
- Subregions of the human MTL can be delineated using individualized imaging
- Human MTL is associated with at least three distributed cortical networks
- Comparison to animal data suggests potentially novel MTL-related pathways in humans

Authors

Daniel Reznik, Robert Trampel, Nikolaus Weiskopf, Menno P. Witter, Christian F. Doeller

Correspondence

reznik@cbs.mpg.de (D.R.), doeller@cbs.mpg.de (C.F.D.)

In brief

Using individualized neuroimaging, Reznik et al. find that different subregions of the human memory system are associated with at least three distributed cortical networks. Comparison to non-human primate connectivity data suggests that some anatomical pathways are potentially not present in humans, some are preserved, and some are potentially new.

Reznik et al., 2023, Neuron *111*, 1–17
September 6, 2023
https://doi.org/10.1016/j.neuron.2023.05.029

CellPress

Please cite this article in press as: Reznik et al., Dissociating distinct cortical networks associated with subregions of the human medial temporal lobe using precision neuroimaging, Neuron (2023), https://doi.org/10.1016/j.neuron.2023.05.029

Neuron

CellPress

Article

Dissociating distinct cortical networks associated with subregions of the human medial temporal lobe using precision neuroimaging

Daniel Reznik,[1,7,*] Robert Trampel,[2] Nikolaus Weiskopf,[2,3] Menno P. Witter,[4] and Christian F. Doeller[1,4,5,6,*]
[1]Department of Psychology, Max Planck Institute for Human Cognitive and Brain Sciences, Leipzig, Germany
[2]Department of Neurophysics, Max Planck Institute for Human Cognitive and Brain Sciences, Leipzig, Germany
[3]Felix Bloch Institute for Solid State Physics, Faculty of Physics and Earth Sciences, Leipzig University, Leipzig, Germany
[4]Kavli Institute for Systems Neuroscience, Centre for Neural Computation, Egil and Pauline Braathen and Fred Kavli Centre for Cortical Microcircuits, Jebsen Centre for Alzheimer's Disease, NTNU Norwegian University of Science and Technology, Trondheim, Norway
[5]Wilhelm Wundt Institute of Psychology, Leipzig University, Leipzig, Germany
[6]Department of Psychology, Technische Universität Dresden, Dresden, Germany
[7]Lead contact
*Correspondence: reznik@cbs.mpg.de (D.R.), doeller@cbs.mpg.de (C.F.D.)
https://doi.org/10.1016/j.neuron.2023.05.029

SUMMARY

Tract-tracing studies in primates indicate that different subregions of the medial temporal lobe (MTL) are connected with multiple brain regions. However, no clear framework defining the distributed anatomy associated with the human MTL exists. This gap in knowledge originates in notoriously low MRI data quality in the anterior human MTL and in group-level blurring of idiosyncratic anatomy between adjacent brain regions, such as entorhinal and perirhinal cortices, and parahippocampal areas TH/TF. Using MRI, we intensively scanned four human individuals and collected whole-brain data with unprecedented MTL signal quality. Following detailed exploration of cortical networks associated with MTL subregions within each individual, we discovered three biologically meaningful networks associated with the entorhinal cortex, perirhinal cortex, and parahippocampal area TH, respectively. Our findings define the anatomical constraints within which human mnemonic functions must operate and are insightful for examining the evolutionary trajectory of the MTL connectivity across species.

INTRODUCTION

Since William Scoville and Brenda Milner described the psychological effects of hippocampal removal in the epileptic patient Henry Molaison, the medial temporal lobe (MTL) has become the focus of research into the neural bases of declarative memory.[1–6] Anatomically, the MTL can be broadly divided into the parahippocampal cortex, perirhinal cortex, and entorhinal cortex that follow the long axis of the parahippocampal gyrus, amygdala, and the hippocampal formation, which includes the dentate gyrus, Ammon's horn, and subicular complex.[7] While the functional role of the MTL for declarative memory is clearly established, its anatomical complexity and heterogeneity inspired multiple debates about potentially unique contributions of its different subregions to mnemonic processes.[8–10]

Animal tract-tracing studies in rodents and non-human primates were tremendously insightful to our understanding of the MTL function and to carefully defining the species-specific anatomical boundaries within which memory-related functions must operate. In particular, tracing studies in the rodent indicate that rodent postrhinal cortex (rodent's homologue to primate parahippocampal cortex) is anatomically connected with the anterior cingulate, retrosplenial, ventral temporal association, and posterior parietal cortex, as well as with the visual and somatosensory association cortex.[11] Rodent's perirhinal cortex, which can be divided into areas 35 and 36, is predominantly connected with the ventral temporal association cortex, piriform cortex, and insular cortex.[12] The entorhinal cortex in the rodent was shown to be anatomically connected with the frontal, insular, parietal, occipital, and temporal cortices.[11,12]

Similar to the rodent, tracing studies in the primate (mostly done on old-world monkeys) indicate as well that distinct subregions of the MTL are anatomically connected with multiple unimodal and polymodal cortices. The primate parahippocampal cortex (which can be divided into areas TH and TF[13,14]) receives direct inputs from the retrosplenial cortex, dorsal bank of the superior temporal sulcus, auditory association cortex in the superior temporal gyrus, posterior portion of parietal lobe (area 7a, including Opt[15]), visual association areas TE/TEO, visual cortex (V4), insula, and frontal lobe, mostly the ventrolateral

and ventromedial parts.[8,16–20] The perirhinal cortex receives direct inputs from the frontal lobe (mostly the ventrolateral and ventromedial parts), dorsal and ventral banks of the superior temporal sulcus, cingulate cortex, visual areas TE/TEO (mostly TE), and insula.[19,20] The entorhinal cortex receives direct inputs from the retrosplenial cortex, cingulate cortex (areas 25, rostral 24, 23, 30, and 32), caudal orbitofrontal cortex, dorsolateral frontal cortex, insula, temporal pole, and superior temporal gyrus, excluding auditory association areas.[21–23] Together with intrinsic connectivity between the MTL substructures (which are not in the focus of the current study), these anatomical findings suggest that the MTL is focal to the integration of significant amount of unimodal and polymodal inputs from the broader neocortex.

Humans shared a common ancestor with old-world monkeys about 25–30 million years ago[24]; therefore, some anatomical homologies exist between macaque brain and human brain.[25–27] However, inferring whole-brain human anatomical connectivity from macaque is challenging due to the disproportional expansion of human cortical mantle (especially of the parietal, frontal, and temporal cortices[28–30]) and the described above anatomical connectivity of different subregions of the macaque MTL can serve only as anatomical *priors* for studying MTL connectivity in humans. Therefore, a detailed anatomical framework of the pathways connecting the human MTL with the broader neocortex is required for understanding the anatomical boundaries of the human memory system.

Since anatomical tract-tracing is unfeasible in humans, other methods have emerged as a proxy to indirectly measure *in vivo* mono- and polysynaptic human neuroanatomical connectivity. One such method is based on recording spontaneous intrinsic brain activity patterns, which proved to be a powerful tool in elucidating the anatomical organization of the brain. For example, on the level of local circuitry, correlations in intrinsic firing patterns reconstruct both the anatomical and functional properties of cats' visual cortex column organization (see Figure 1 in Kenet et al.[31]). On the macro-, large-scale organization level, intrinsic brain activity can be estimated by measuring blood oxygenation level-dependent (BOLD) signal with functional magnetic resonance imaging (fMRI) during spontaneous brain activity. Using the recorded BOLD signal over time, it is then possible to calculate correlation patterns in spontaneous activity between distributed brain regions[32] to reveal functional and anatomical organizational properties at the whole-brain level.[33–36] More specifically, distributed brain networks in non-human primates estimated by correlations in low-frequency spontaneous brain activity closely followed the same networks estimated by anatomical tract-tracing in the macaque[37] and in the marmoset.[38] Taken together, BOLD fMRI functional connectivity patterns serve as a powerful means to noninvasively estimate large-scale anatomical connectivity.

Previous human fMRI studies used functional connectivity methods to explore how different subregions of the MTL (more specifically, the parahippocampal, perirhinal, and entorhinal cortices) are connected with rest of the brain.[39–46] While most of these studies were able to reproduce some of the anatomical priors related to the parahippocampal cortex (based on macaque MTL connectivity), whole-brain connectivity findings pertaining to the entorhinal and perirhinal cortices, situated in the anterior portion of the MTL, were mixed and only minimally compliant with the primate tract-tracing hypotheses (but see Maass et al.[47] for a detailed connectivity exploration within the MTL). Additional human connectivity data which do not comply with known monkey anatomy pertain to parahippocampal areas TH/TF[48,49] that in human MRI studies are typically considered together to constitute the parahippocampal cortex.

One can argue that during the course of cortical expansion, some anatomical pathways present in non-human primates were changed in humans.[50] While this is of course a possibility, we nevertheless believe that at least two potential reasons prevented a thorough and detailed exploration of human entorhinal and perirhinal cortices, and parahippocampal areas TH/TF; therefore, important connectivity features of subregions of the human MTL with the broader neocortex still await discovery. *First*, the entorhinal and perirhinal cortices are located in the anterior portion of the MTL. This brain region is located just above the petrous part of the temporal bones and very close to the sphenoid sinuses.[40] Therefore, this region is strongly affected by susceptibility artifacts leading to signal loss and geometric distortion in fMRI. Consequently, data quality in the entorhinal and perirhinal cortices (typically measured by temporal signal-to-noise ratio, tSNR) is extremely low, as opposed to in the more posterior portion of the MTL where the parahippocampal cortex is situated. *Second*, the entorhinal and perirhinal cortices, as well as parahippocampal areas TH/TF, are located in close vicinity to each other. The cytoarchitectonic boundary between the entorhinal and perirhinal cortices depends on the depth of the collateral sulcus, which differs across individuals[51,52]; and parahippocampal areas TH/TF occupy the anatomically adjacent banks of the collateral sulcus. Therefore, using group averaged data, where fine anatomical details are blurred across individuals, it is challenging to confidently define the boundary between the entorhinal and perirhinal cortices, and between parahippocampal areas TH/TF (e.g., see Kahn et al.[40] for mixed entorhinal/perirhinal seeds). Even though early fMRI studies were focused on individual subjects (as a historical continuation of animal lesion and tract-tracing research), only recently within-individual, precision neuroimaging approaches were applied to whole-brain cortical mapping, providing invaluable insights into the functional and anatomical architecture of the human brain.[53–60]

To overcome these challenges and to explore in detail the whole-brain cortical topography associated with subregions of the human MTL, we repeatedly scanned four individuals to collect for each around 4 h of high-quality fixation task data ("resting-state"). Within-subject data collection, processing and analysis was inspired by recent precision neuroimaging studies focusing on small samples of densely sampled individuals.[53–58,60] After dividing the fMRI data collected in each individual into discovery and independent validation datasets, we were able to reliably dissociate at least three distributed cortical networks associated with the parahippocampal, entorhinal, and perirhinal cortices.

Please cite this article in press as: Reznik et al., Dissociating distinct cortical networks associated with subregions of the human medial temporal lobe using precision neuroimaging, Neuron (2023), https://doi.org/10.1016/j.neuron.2023.05.029

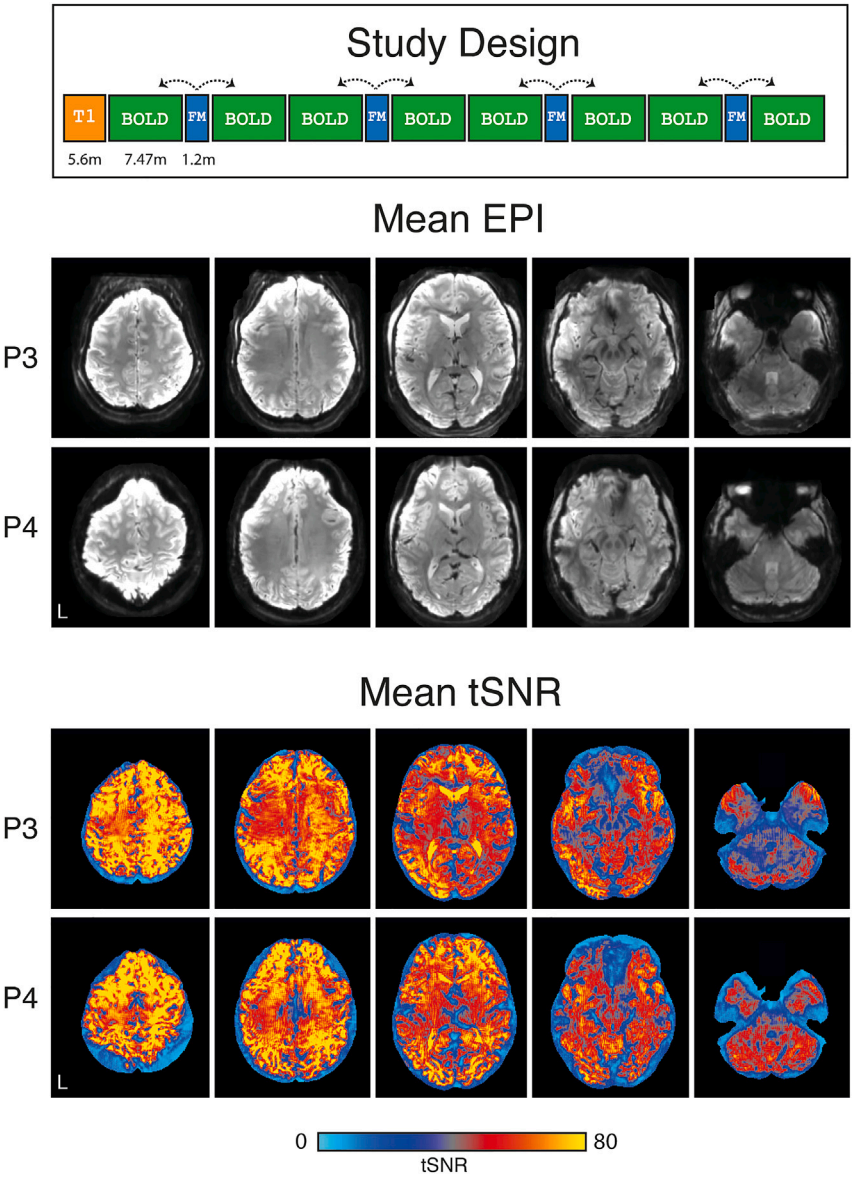

Figure 1. Study design and data quality

Top—experimental design. Each participant was scanned during 4 MRI sessions (first scanning session is depicted here graphically). Each session comprised 8 fixation task runs (BOLD) and 4 field map scans (FM). During the first session, a structural T1-weighted scan was acquired for each participant. The field map scans were collected throughout the scanning sessions and were interleaved with the fixation task runs such that each field map was used to unwarp the temporality adjacent BOLD runs (marked with arrows). Overall, ~240 min of BOLD data were acquired for each participant. *Middle and bottom*—axial slices from P3 and P4 showing mean BOLD (*middle*) and mean tSNR (*bottom*) data. High coverage and high tSNR were obtained in most regions of the brain, particularly in the medial temporal lobe. Note the relatively lower data quality in the ventral portions of the medial prefrontal cortex and the lateral surface of the temporal lobes. See Figure S1 for the same data from P1 and P2. Left (L) refers to left hemisphere.

RESULTS

Data quality in densely sampled individuals

Participants (n = 4) performed a fixation task, which is notoriously difficult to perform for long periods of time due to its monotonicity, associated with participants' fatigue and increased head movement (alternatives were proposed almost a decade ago by Krienen et al.[61] and recently re-emerged[62]). Nevertheless, all our participants were compliant and showed very little head movement. We had to exclude only one BOLD run out of total 128 runs across all participants. Maximum absolute head displacement for P1 ("P" stands for participant) was 1.6 mm, for P2 0.62 mm, for P3 1.9 mm, and for P4 1.2 mm (after excluding one BOLD run with maximum movement of 2.9 mm). In every participant, no difference in head motion between discovery and validation datasets was observed (all t test $p < 0.23$). Mean BOLD data and mean tSNR maps for 2 example participants P3 and P4 can be seen in Figure 1 (see Figure S1 for data from the other 2 participants and Figure S2B for coronal tSNR slices). High coverage and high tSNR values were achieved in nearly all brain regions, including the MTL. More specifically, the mean tSNR for anterior MTL seeds across participants was 43.9 (unsmoothed data). Compared with the vast majority of previous studies that performed whole-brain 2D EPI imaging and explicitly reported tSNR in these regions (e.g., tSNR of ~11.5[63]; tSNR of 11[64]; tSNR of ~8[65]; tSNR of ~10[44]; also see tSNR of 43[66]), our study provides excellent data quality in these notoriously challenging-to-image brain regions, allowing robust estimation of the distributed brain networks associated with subregions of the MTL, and particularly the anterior MTL. Parahippocampal, entorhinal, and perirhinal seeds for two example participants are shown in Figure 2 both on BOLD and T1 images (marked with cyan asterisk; see Figure S2A for data from the other 2 participants).

Distinct brain anatomy associated with subregions of the MTL: Discovery

The goal of the current study was to explore the cortical brain regions associated with distinct subregions of the human MTL within individuals. For each participant, we explored the discovery dataset (half of the data for each participant) and put seeds throughout the parahippocampal gyrus and collateral sulcus to discover the whole-brain correlation patterns linked to their different regions. The associations between different seeds

Please cite this article in press as: Reznik et al., Dissociating distinct cortical networks associated with subregions of the human medial temporal lobe using precision neuroimaging, Neuron (2023), https://doi.org/10.1016/j.neuron.2023.05.029

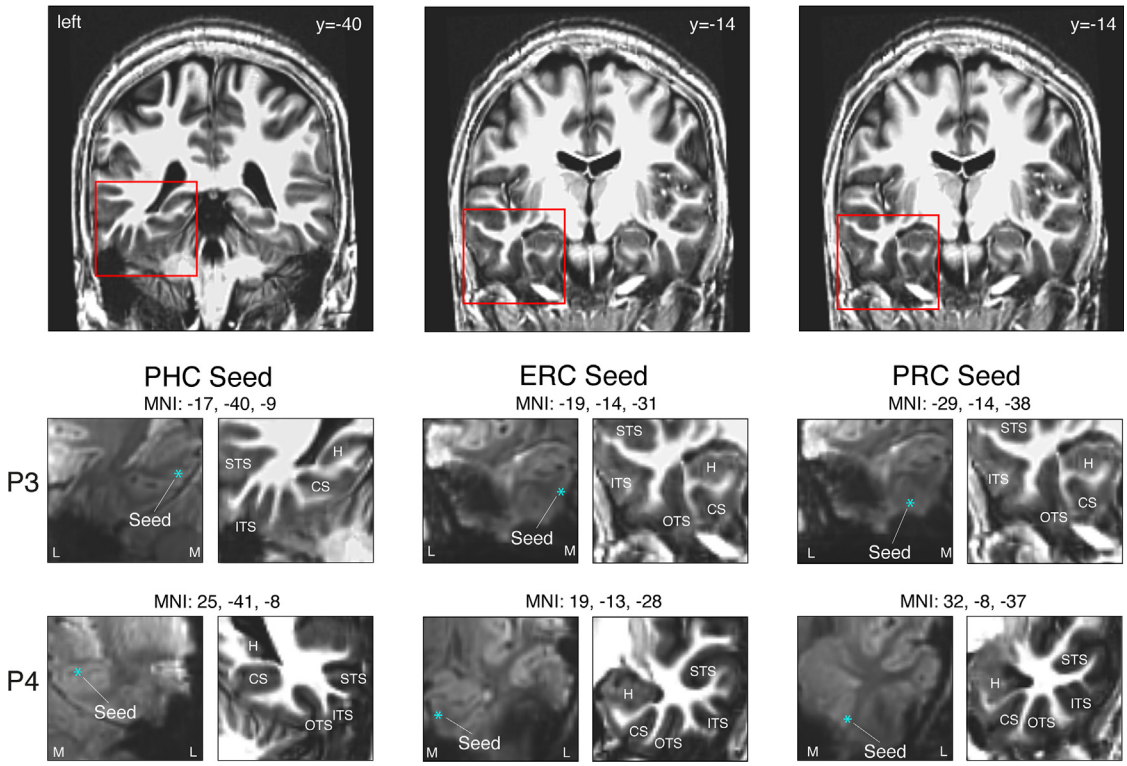

Figure 2. Seed regions in the MTL

Coronal slices of the medial temporal lobe from P3 and P4 showing the seed regions in the parahippocampal (area TH, PHC), entorhinal (ERC), and perirhinal (PRC) cortices on T1 and mean BOLD data, respectively (seeds are marked with cyan asterisks). Note excellent coverage of the perirhinal and entorhinal cortices. See Figure S2A for the same data from P1 and P2. M, medial; L, lateral.

and whole-brain correlation patterns found in the discovery datasets were then blindly tested using independent validation datasets (other half of the data).

Correlation maps associated with parahippocampal area TH are shown in Figure 3, left column. In all 4 participants, a seed located in the posterior portion of the parahippocampal gyrus correlated with an area which we consider to be the retrosplenial cortex (since it occupied the ventral part of the posteromedial cortex, potentially corresponding to BA29 and BA30), dorsal precuneus, caudal portion of the inferior parietal lobule, ventral medial prefrontal cortex (involving areas BA24, BA32, and BA10[26]), and dorsolateral prefrontal cortex. Overall, the distributed brain regions that were associated with parahippocampal area TH corresponded to the spatial topography of one subdivision of the canonical default network, known as default network A.[53–55]

Correlation maps associated with the entorhinal cortex (most likely, with its posterior portion; see discussion) are shown in Figure 3, middle column. Seeds located in the anterior medial portion of the parahippocampal gyrus showed consistent correlations patterns across all 4 participants and included the posterior cingulate cortex, rostral inferior parietal lobule, large portions of the lateral temporal cortex extending to the temporal pole, ventral and dorsal medial prefrontal cortex (involving areas BA24, BA32, and BA10[26]), and dorsolateral prefrontal cortex. Overall, the correlation patterns of the entorhinal cortex followed the spatial topography of another subdivision of the canonical default network, known as default network B.[54]

Correlation maps associated with the perirhinal cortex are shown in Figure 3, right column. Seeds located in the lateral bank of the anterior portion of the collateral sulcus correlated with the extrastriate cortex (area anterior to the middle temporal area complex MT+), dorsal caudal frontal cortex (in or around the frontal eye field), ventral caudal frontal cortex, superior parietal lobule, central portion of the anterior-posterior extent of the cingulate gyrus, and the rostral portion of the inferior frontal gyrus. We assumed that the correlations with the extrastriate cortex are likely to correspond to the area anterior to MT+ for two reasons. First, this area was shown to strongly correlate with a similar distributed brain network reported in Yeo, Krienen et al.[67] Second, in all participants, peak correlations with the perirhinal cortex in that area were located rostrally to the peak coordinate of 143 studies localizing the human area MT (NeuroSynth tool[68]), corresponding to the relative anatomical location of the area anterior to MT+ and MT+. Overall, the correlation patterns with the perirhinal cortex corresponded to the spatial topography of the dorsal attention network[69] and specifically, to its subdivision A[54,67] (see formal analyses below).

Even though our seeds were positioned in one hemisphere, the correlation maps for each MTL seed were mostly symmetric across two hemispheres (see Figure S3 for unthresholded maps). Consistency of these correlation patterns across all

Please cite this article in press as: Reznik et al., Dissociating distinct cortical networks associated with subregions of the human medial temporal lobe using precision neuroimaging, Neuron (2023), https://doi.org/10.1016/j.neuron.2023.05.029

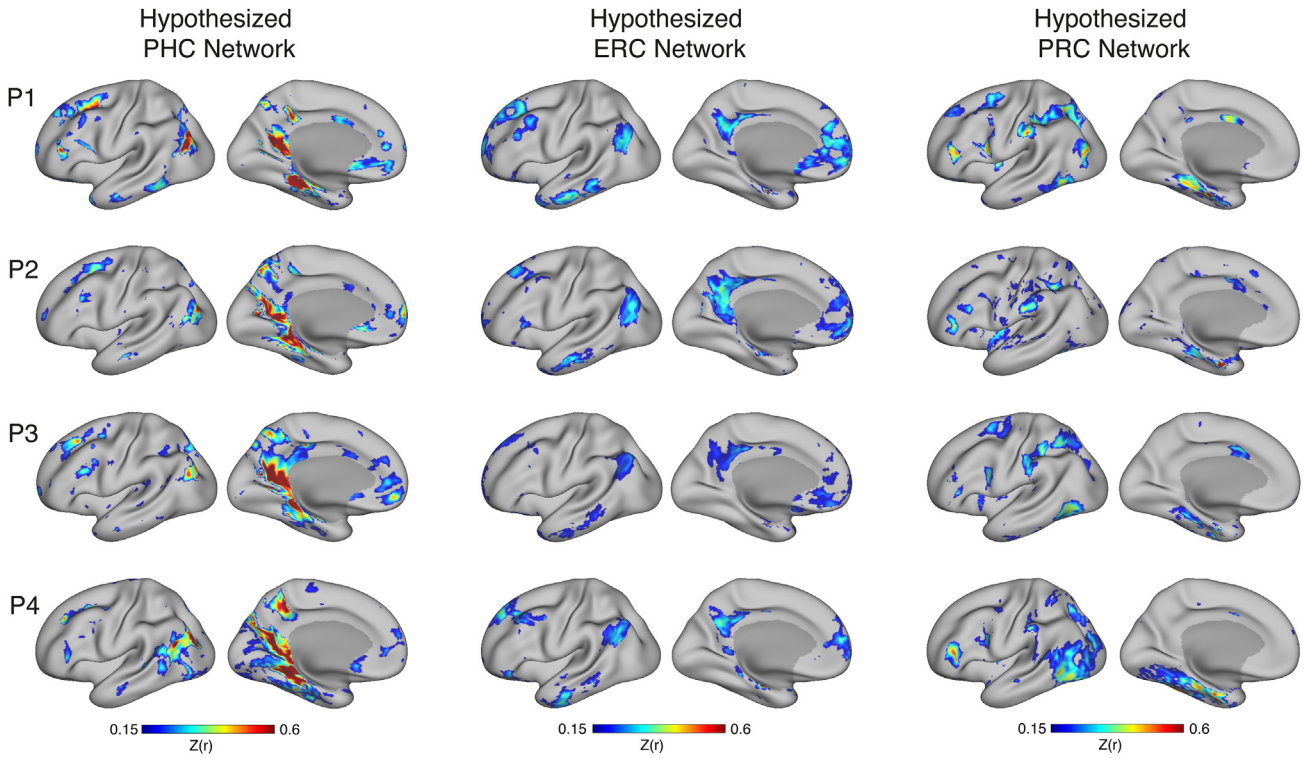

Figure 3. Subregions of the MTL are associated with distinct cortical networks

Surface-projected functional connectivity maps produced for each MTL seed region in each participant using the discovery datasets. Each row shows connectivity maps from each participant (P1–P4), and each column shows connectivity maps from each MTL seed. Seeds placed in the parahippocampal cortex (area TH, PHC) were associated with a hypothesized distributed brain network that follows the topography of one subdivision of the default network. Seeds placed in the entorhinal cortex (ERC) were associated with a hypothesized distributed brain network that follows the topography of another subdivision of the default network. Seeds placed in the perirhinal cortex (PRC) were associated with a hypothesized distributed brain network that follows the topography of one subdivision of the dorsal attention network. Some surface images were right-to-left flipped to match the presented orientation across participants for clearer comparison of the displayed topographies. Connectivity maps were thresholded above the noise correlation level (z(r) > 0.15). Note the consistency across participants and the multiple dissociations across the cortex between different seed regions.

participants provided a strong hypothesis for at least three distinct networks that are associated with the human MTL. The correlation maps were largely non-overlapping and importantly, the whole-brain correlation maps were not contingent on a particular seed location and were replicable with multiple seed voxels from each MTL subregion that were moved around the reported seed location (Videos S1, S2, S3, S4, and S5). Finally, connectivity maps showed high stability across discovery and validation datasets with minimum Pearson correlation coefficient of 0.81 (all $p < 0.001$) across participants and MTL subregions.

Distinct brain anatomy associated with subregions of the MTL: Validation

The results of the discovery analysis provided us with the hypotheses that distinct subregions of the human MTL are associated with distinct cortical networks. Next, using independent validation datasets, we blindly tested these hypotheses and examined whether networks revealed during the discovery analyses are indeed associated with distinct subregions of the MTL. During the validation analyses, we tested four different brain regions that showed anatomically close correlations with the entorhinal cortex, perirhinal cortex, and parahippocampal area TH in each participant. The regions were the parietal lobe, superior frontal gyrus, posteromedial cortex, and ventromedial prefrontal cortex. In each region, using the discovery datasets, we selected seeds that maximally correlated (using a Fisher z-transformed Pearson correlation coefficient) with distinct subregions of the MTL (see top row in Figure 4 for appreciating the general anatomical proximity between the dissociation seeds). It is important to emphasize that all seeds were *a priori* selected using *only* the discovery datasets and then used for the validation analyses. For every seed located in each of the four cortical dissociation regions, a Fisher z-transformed Pearson correlation map was calculated for each participant, and we then examined the "back-projection" correlation values with the MTL seed regions. All ANOVA were significant (all F-values > 9.4 and all ps < 0.01; Figure 4), and all participants showed crossover effects where relevant. These validation findings replicated the correlation patterns with distinct subregions of the MTL we observed during the discovery analysis and statistically dissociated connections of multiple cortical regions with the human entorhinal cortex, perirhinal cortex, and parahippocampal area TH (see Figure S6A for testing other cortical brain regions that showed correlations only with one subregion of the MTL). To

Please cite this article in press as: Reznik et al., Dissociating distinct cortical networks associated with subregions of the human medial temporal lobe using precision neuroimaging, Neuron (2023), https://doi.org/10.1016/j.neuron.2023.05.029

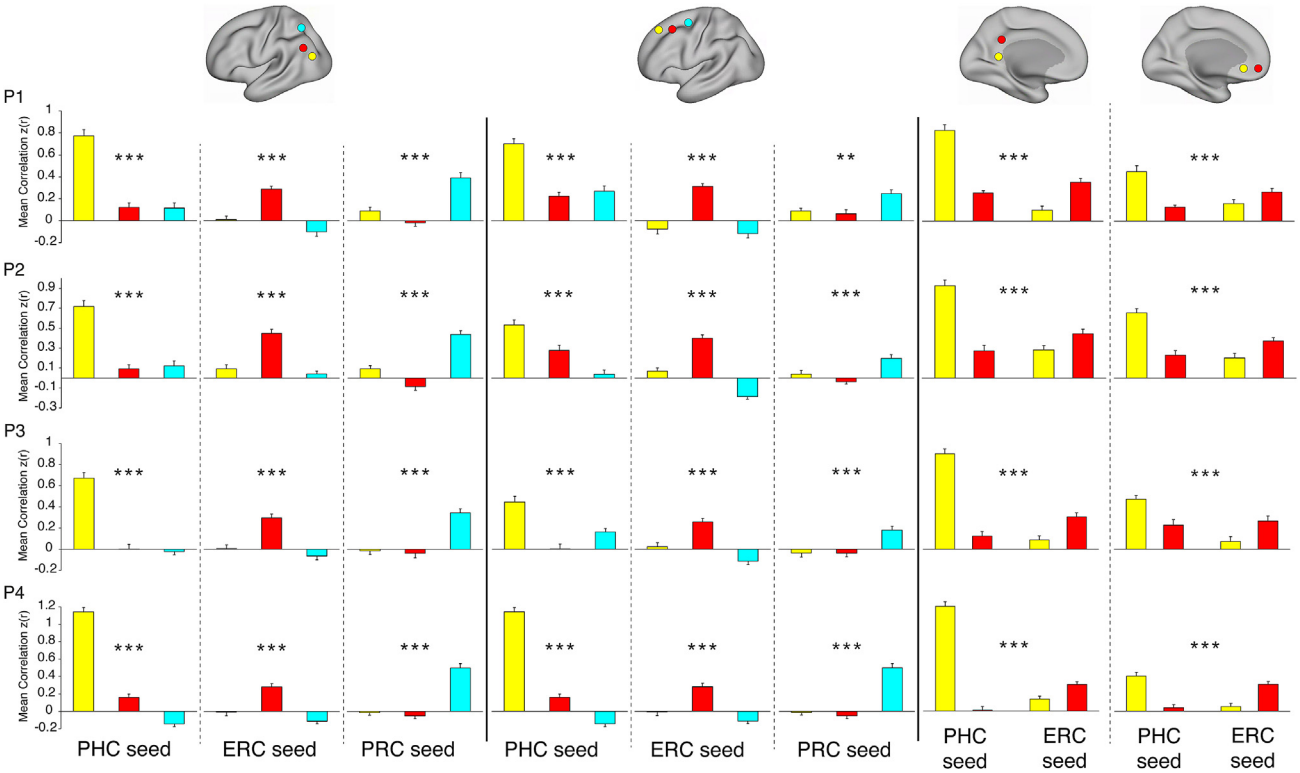

Figure 4. Cortical networks associated with subregions of the MTL are statistically dissociated using independent validation datasets

We calculated "back-projections" connectivity maps seeding from regions in the parietal lobe, dorsolateral frontal cortex, posteromedial cortex, and ventral medial prefrontal cortex and examined the correlation strength in each subregion of the MTL. All cortical and MTL seeds were *a priori* selected using the discovery datasets. Using independent validation datasets, we showed that distinct regions distributed across the cortex differently correlated with distinct subregions of the MTL, and these distinctions were statistically significant (all $p < 0.01$). Bars are mean correlations across all available validation dataset runs ± SEM. Representative example seeds are shown on a surface representation at the top. See also Figure S6A for a similar analysis of cortical regions that did not show close correlations with multiple MTL subregions. $^{**}p < 0.01$, $^{***}p < 0.001$.

conclude, the reported dissociations across the cortex provided robust support that subregions of the MTL are indeed associated with distinct cortical networks within individuals.

Above and beyond the formal statistical testing, another support for the claim that distinct subregions of the MTL are associated with distinct cortical networks was the spatial correlation patterns revealed with analyzing the validation datasets. As can be seen in two example participants (Figure 5—P3 and P4), "back projections" from distinct regions in the parietal lobe revealed not only the full extent of the cortical networks associated with them, but also strong bilateral correlations with distinct regions of the MTL, anatomically corresponding to the entorhinal, perirhinal, and parahippocampal cortex (see two more participants in Figure S4A).

To our surprise, one unexpected finding emerged after we visually inspected these "back projection" correlations. We found that the "back projections" from the caudal and rostral inferior parietal lobule occupied neighboring regions in the anterior medial portion of the parahippocampal gyrus. More specifically, "back projections" from the rostral inferior parietal lobule occupied more ventral portions of the parahippocampal gyrus (anatomically corresponding to the entorhinal cortex), and the "back projections" from the caudal inferior parietal lobule occupied more dorsal portions of the parahippocampal gyrus, only a few millimeters away (anatomically corresponding to the subicular complex, and due to the distal location, we assume this is likely to be the pre/parasubiculum; see correlations separated by the white line in Figures 5 and S4A). We explored this striking distinction by using the best connectivity estimate comprising all available BOLD scans for each participant and placed new seeds within the putative pre/parasubiculum and the putative entorhinal cortex, identified as the maximum connectivity estimates within these regions with the parietal lobe seeds that could be localized on the same coronal slice. In Figure 6A, we highlight P3 and P4 and show that seeds located only a few millimeters apart in the entorhinal cortex and pre/parasubiculum are associated with distinct cortical topography. Note that the pre/parasubiculum correlations mostly correspond to correlations produced by seeds positioned in parahippocampal area TH.

One more unexpected finding emerged from examining "back projections" in the parahippocampal cortex. We found that "back projections" from the superior parietal lobe (perirhinal network) occupied the lateral bank of the part of the collateral sulcus where we localize at least parts of the parahippocampal

Please cite this article in press as: Reznik et al., Dissociating distinct cortical networks associated with subregions of the human medial temporal lobe using precision neuroimaging, Neuron (2023), https://doi.org/10.1016/j.neuron.2023.05.029

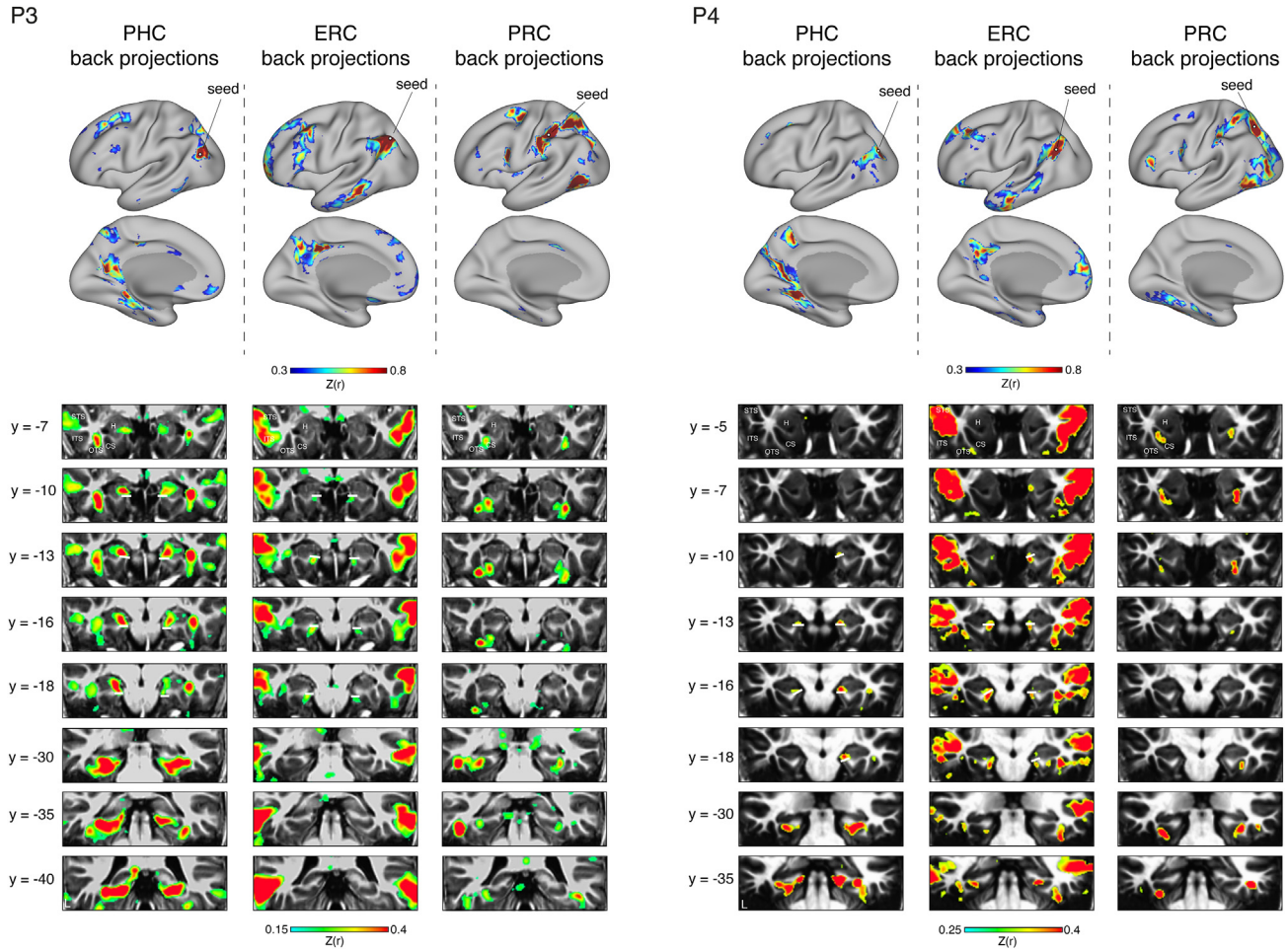

Figure 5. Back projections from parietal cortex seeds—P3 and P4

Top—surface-projected functional connectivity maps produced for each parietal lobe seed in P3 and P4 using the validation datasets. *Bottom*—coronal slices through the MTL showing correlations with the parietal lobe seeds. Note the bilaterally distinct connectivity patterns in the MTL for different parietal lobe seeds. Also note the distinct connectivity patterns in the anterior MTL separated by the white line. The maps were thresholded within participants to best capture the differences in connectivity patterns. See Figure S4A for the same data from P1 and P2 and Figure S4B for "back projections" from other cortical regions highlighting P3 and P4.

cortex. On the other hand, ''back projections'' from the caudal inferior parietal lobule (parahippocampal area TH network) occupied the sulcus' medial bank (corresponding to parahippocampal area TH). We could not confidently identify distinct seeds along both banks of the posterior collateral sulcus that were consistently associated with distinct networks in all participants (possibly due to spatial smoothing and mixture of signals within the walls of the sulcus; Videos S3 and S4). Therefore, we pursued this exploratory observation by calculating connectivity differences between the retrosplenial cortex and the area anterior to MT+, defined as the maximum correlation value across all available BOLD scans with the caudal inferior parietal lobule and superior parietal lobule, respectively. In Figure 6B, we highlight P3 and P4 that show the dissociation between the medial portion of the posterior collateral sulcus (potentially corresponding to area TH) and its lateral portion (potentially corresponding to area TF; see discussion). In P1 (Figure S5), the connectivity associated with the area anterior to MT+ extended laterally all the way into the fusiform gyrus, similarly to the parcellation of parahippocampal areas TH/TF proposed by von Economo and Koskinas.[13]

Finally, we explored the possibility that the distributed cortical network associated with the perirhinal cortex corresponds to one subdivision of the dorsal attention network. To this end, we identified the other subdivision of the dorsal attention network[67] (which later was referred to as the subdivision B in Braga and Buckner[54]) by placing seeds in the middle occipital collateral sulcus[70] (see STAR Methods) and examined its association with the MTL subregions. Figure 7A displays the cortical projection of the distributed brain regions associated with the occipital collateral sulcus (right column) and the ''back-projections'' from the superior parietal lobule associated with the perirhinal cortex (left column). Because the peaks of these two networks had little or no overlap and their joint

Please cite this article in press as: Reznik et al., Dissociating distinct cortical networks associated with subregions of the human medial temporal lobe using precision neuroimaging, Neuron (2023), https://doi.org/10.1016/j.neuron.2023.05.029

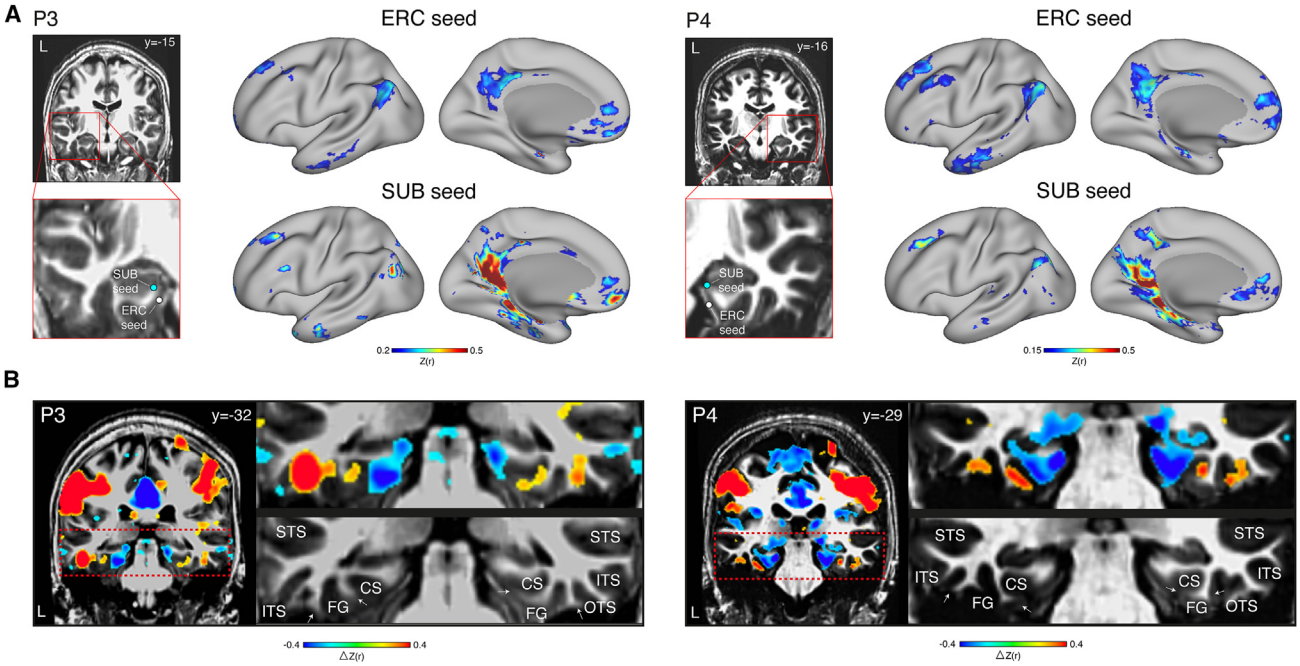

Figure 6. Exploratory analyses

(A) The entorhinal cortex and pre/parasubiculum are associated with distinct cortical networks. Seeds placed only a few millimeters apart in the entorhinal cortex (ERC, white circles) and pre/parasubiculum (SUB, cyan circles) were associated with distinct cortical networks. This exploratory analysis highlighting P3 and P4 suggests that the distributed brain network associated with the subicular complex is similar to the distributed brain network associated with parahippocampal area TH.

(B) Different subregions of the parahippocampal cortex are differentially associated with the retrosplenial cortex and the area anterior to MT+ in P3 and P4. While the medial bank of the collateral sulcus (anatomically corresponding to parahippocampal area TH) was more strongly associated with the retrosplenial cortex (blue), the lateral bank of the collateral sulcus (anatomically corresponding to parahippocampal area TF) was more strongly associated with the area anterior to MT+ (red). See Figure S5 for data from P1. In both panels the maps were thresholded within participants to best capture the differences in connectivity patters.

topography followed closely the canonical dorsal attention network, we concluded that the set of distributed brain regions associated with the occipital collateral sulcus was indeed capturing the subdivision B of the dorsal attention network. As can be seen in Figure 7B, the subdivisions A and B of the dorsal attention network were dissociated in all four participants. P4 showed consistent connectivity nearly in the entire longitudinal axis of the lateral bank of the collateral sulcus with the subdivision B of the dorsal attention network; however, this connectivity pattern was not present in other participants, and the connectivity values were much smaller compared to connectivity values with the perirhinal network. Importantly, the maximum correlation value across all participants between the seeds from the putative subdivision B of the dorsal attention network and other MTL subregions was z(r) = 0.03 (suspected parahippocampal area TH of P4).

DISCUSSION

In the current study, we explored the cortical pathways associated with the human entorhinal cortex, perirhinal cortex, and parahippocampal area TH using intrinsic functional connectivity in densely sampled individuals. Our results indicate that the cortical network associated with parahippocampal area TH follows the distributed topography of one subdivision of the default network, known as the subdivision A.[36,53,54,71] The cortical network associated with the entorhinal cortex follows the distributed topography of a different subdivision of the default network, known as the subdivision B.[40,41,53,54,71] The cortical network associated with the perirhinal cortex follows the distributed topography of the subdivision A of the dorsal attention network.[54,67,69]

Relations to prior studies

Previous human group-level studies that addressed a similar question were only partially able to characterize the distributed brain anatomy associated with the medial temporal lobe. For example, the pioneer studies by Kahn et al.[40] and Libby et al.[41] found that human parahippocampal cortex is associated with the posterior midline cortical areas (without making the distinction between the posterior cingulate and potential retrosplenial cortex), inferior parietal lobe (without making the distinction between its subparts), and ventral medial prefrontal cortex. Furthermore, in these studies, human perirhinal/entorhinal cortex is associated with the lateral surface of the temporal lobe and lateral frontal cortex. The study by Wang et al.[46] examined further the associations of the anterior perirhinal cortex and reported a set of distributed brain regions resembling the perirhinal networks we report in our study.

These and other past group-level studies set the foundation for the classical view on human MTL connectivity with the

Please cite this article in press as: Reznik et al., Dissociating distinct cortical networks associated with subregions of the human medial temporal lobe using precision neuroimaging, Neuron (2023), https://doi.org/10.1016/j.neuron.2023.05.029

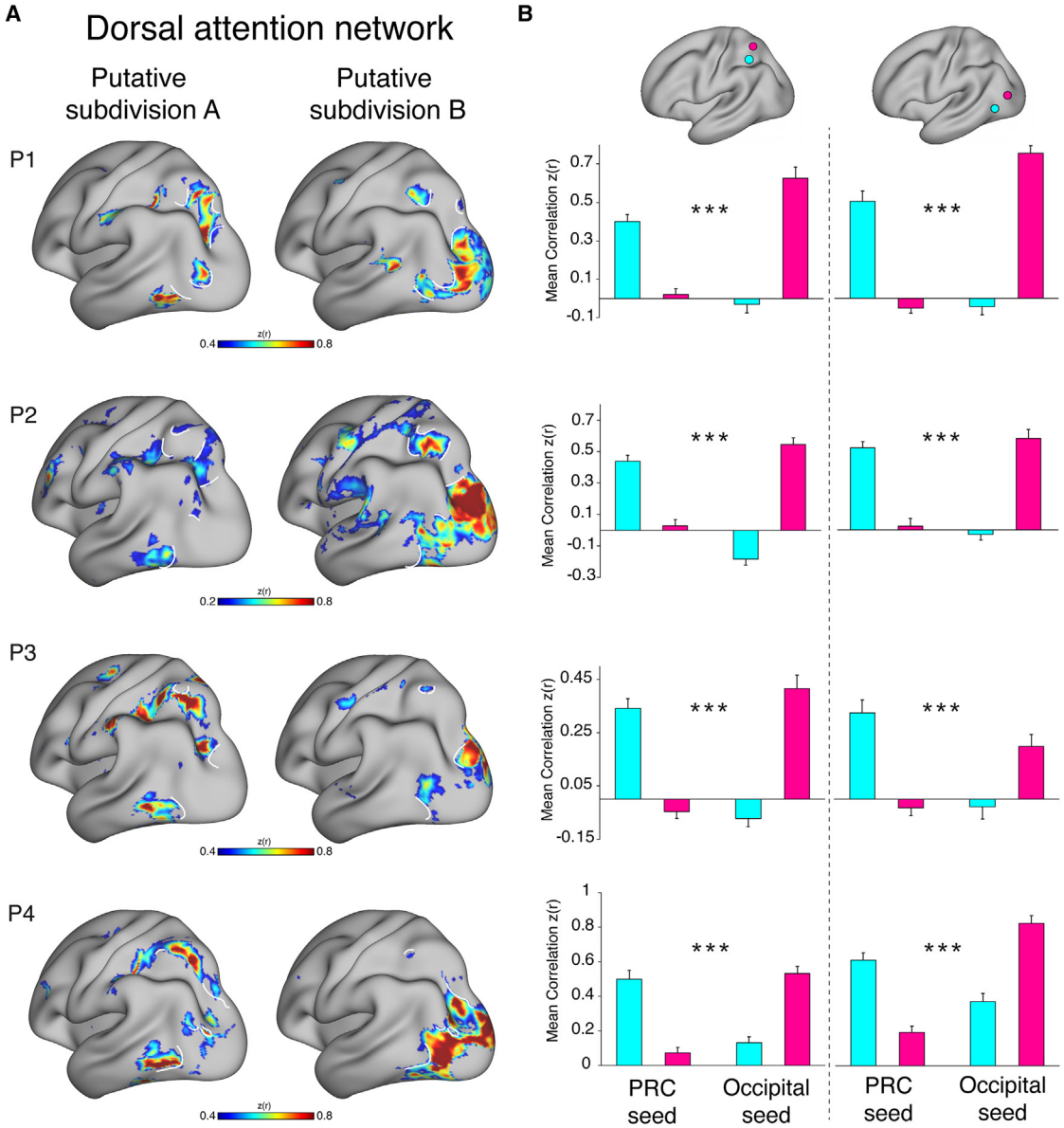

Figure 7. Dissociating two putative subdivisions of the dorsal attention network

(A) Cortical projections of the connectivity maps generated by seeding the region in the superior parietal lobe that correlated with the perirhinal cortex (left column) and the middle portion of the occipital collateral sulcus (right column).

(B) The two putative subdivisions A and B of the canonical dorsal attention networks are dissociable in respect to their connectivity with the MTL. While the MTL-related subdivision A was associated with the perirhinal cortex, at least parts of the subdivision B were not (all $p < 0.001$). Representative example seeds from the two putative subdivisions of the canonical dorsal attention networks are shown on a surface representation at the top. Bars are mean correlations across all available validation dataset runs ± SEM, ***$p < 0.001$.

broader neocortex postulating that there are two pathways associated with human perirhinal/entorhinal and parahippocampal cortices—the anterior pathway and the posterior pathway.[9,10,40,41] Our precision neuroimaging results can account for this view, as the brain regions that were previously reported to constitute the anterior and posterior pathways have partial correspondence to the distributed brain networks we found to be associated with subregions of the MTL within individuals. The anterior pathway has topographical components, such as the lateral temporal lobe and superior parietal lobule, that are a mixture of brain regions that are parts of the networks associated with the entorhinal cortex (lateral temporal lobe) and perirhinal cortex (superior parietal lobule[46]). The posterior pathway has multiple components that overlap with brain regions that are parts of the network associated with the parahippocampal area TH, such as the posteromedial cortex and inferior parietal lobule.[40] In our study, we could explore important anatomical details, such as the boundary

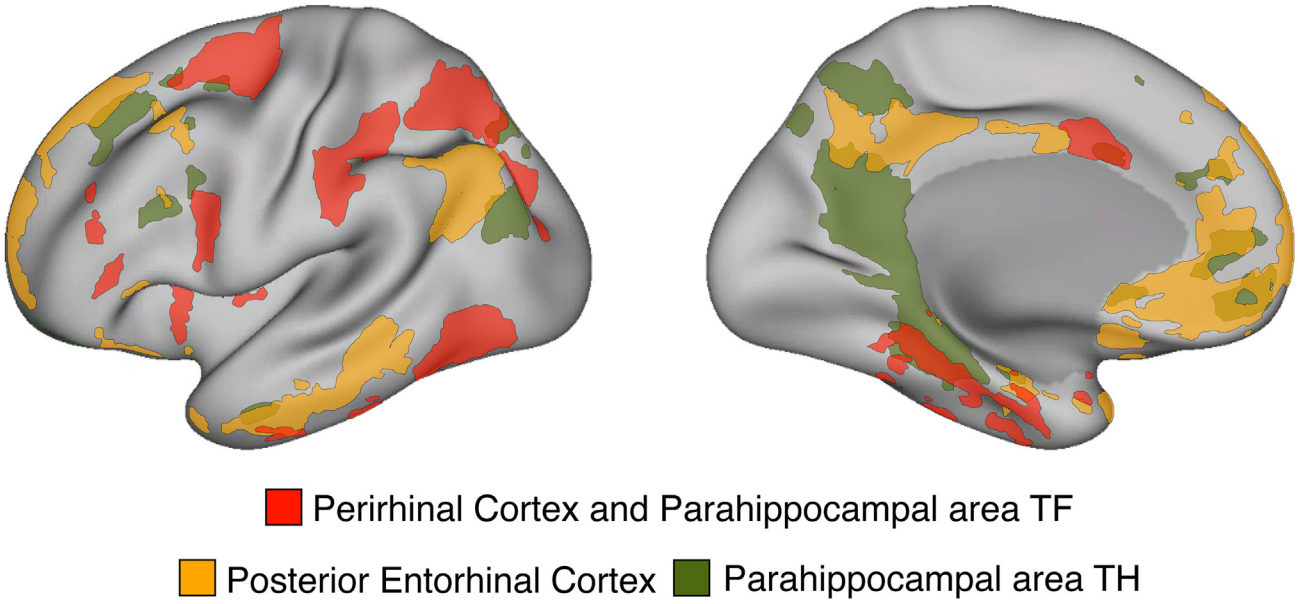

Figure 8. Subregions of the human MTL are associated with distinct distributed cortical networks

A cortical surface map showing a schematic whole-brain neuroanatomical architecture of the distributed cortical networks associated with subregions of the human medial temporal lobe. See also Figure S8.

between the entorhinal and perirhinal cortices, and the separation between parahippocampal areas TH/TF. Consequently, our findings substantially extend and complement previous group-level reports by showing that instead of the canonical two-pathways system, there are at least three distinct cortical networks linked to the human parahippocampal area TH, entorhinal cortex, and perirhinal cortex (Figure 8). Moreover, our findings put the human MTL connectivity with the broader neocortex in a strict biologically driven anatomical context, allowing insightful comparisons between animal and human data.

Distributed cortical networks associated with the human MTL are compliant with monkey anatomy

The three networks that we found to be associated with distinct regions of the human MTL are consistent with multiple anatomical priors expected from monkey tracing studies, but differ in a way that provides striking anatomical insights into the evolutionary trajectory of cortical development supporting memory functions in humans.

We found that the human parahippocampal area TH is preferably associated with the retrosplenial cortex rather than with the posterior cingulate cortex. The entorhinal cortex connectivity with the posteromedial cortex was complementary in that the entorhinal cortex showed preferred connectivity with the posterior cingulate cortex compared with the retrosplenial cortex. This dissociation is intriguing given monkey anatomy showing that the parahippocampal and entorhinal cortices are anatomically connected *both* with the retrosplenial cortex and posterior cingulate cortex.[18,23,72,73] We found that the human perirhinal cortex connections with the posteromedial cortex were minute (the topography of the perirhinal network revealed no connectivity patterns with these brain area), which is consistent with monkey anatomy showing minimal anatomical connectivity between these regions.[19,20]

Another key dissociation was found in the parietal lobe. We found that the human parahippocampal area TH and entorhinal cortex are preferably connected with different segments of the posterior inferior parietal lobule. While parahippocampal area TH has stronger connections with the more caudal portion of the posterior inferior parietal lobule, the entorhinal cortex is more strongly connected with the more rostrally situated portion. Connectivity of parahippocampal area TH with the parietal lobule is consistent with monkey anatomy showing that monkey parahippocampal cortex shares anatomical connections with the posterior portion of the inferior parietal lobe (area 7a and Opt[19,20,74]). Similarly, monkey entorhinal cortex has anatomical connectivity (albeit weak) with the inferior parietal lobe.[75,76] We found that the human perirhinal cortex was not associated with the inferior parietal lobule, which is consistent with tract-tracing injections in the monkey.[19,20] However, large injections in the inferior parietal cortex that included areas 7b and 7a (excluding the most posterior 7a area Opt) in monkeys indicate connectivity with the perirhinal cortex.[74,77] Our data suggest that the human perirhinal cortex is connected with the superior parietal lobule. Given the significant expansion of the human parietal cortex compared with monkeys, it was suggested that the human homologue of monkey inferior parietal area 7b has shifted dorsally to occupy the superior parietal lobule.[29] Though currently speculative, this notion can account for the connectivity we observed between the human perirhinal cortex and parietal lobe.

Connections with the lateral surface of the temporal lobe also showed differential connectivity patterns with the human parahippocampal, entorhinal, and perirhinal cortices. We found that

the entorhinal cortex was heavily connected with the temporal pole and almost the entire rostro-caudal extent of the middle temporal gyrus. Parahippocampal area TH connections with the lateral surface of the temporal lobe were inconsistent across participants and included only its small rostral portion. The perirhinal cortex connections with the rostral and lateral surface of the temporal lobe were minute; however, we observed that the perirhinal cortex was associated with the area anterior to MT+. Compared with the monkey anatomy, our findings are consistent with the known entorhinal cortex connectivity with the temporal pole and the entire rostro-caudal axis of the lateral temporal lobe sparing the visual areas in the inferior temporal lobe (areas TE/TEO). However, unlike in monkeys, we observed no consistent connections of neither of the MTL subregions with the superior temporal gyrus (see Figure S6B for formal analyses). Together with the parietal cortex, the lateral temporal cortex has experienced significant expansion in humans. Potential outcomes of such expansion were dramatic development of auditory association areas in the superior temporal gyrus and significant shift of visual areas to ventral-posterior portions of the temporal lobe.[78]

Medial and lateral surfaces of the frontal lobe also showed interesting connectivity dissociations with the human parahippocampal, entorhinal, and perirhinal cortices. While both parahippocampal area TH and the entorhinal cortex were associated with the ventral medial prefrontal cortex, the entorhinal cortex was associated with the dorsal medial prefrontal cortex extending to the superior frontal gyrus. Parahippocampal area TH, on the other hand, had more modest connections with the dorsolateral surface of the frontal lobe. These findings are broadly consistent with the monkey tract-tracing data showing that monkey parahippocampal and entorhinal cortices are anatomically connected with the medial and lateral frontal cortices. However, and inconsistent with our findings, monkey entorhinal cortex is only lightly connected with the dorsolateral frontal cortex.[22] Monkey perirhinal cortex connectivity with the frontal cortex is rather weak, and it is mostly associated with areas 11, 12, and 13.[20] Our findings indicate that the network associated with the human perirhinal cortex did not include the medial prefrontal cortex but spanned the most ventral areas of the inferior frontal gyrus (corresponding anatomically to frontal area 47, a proposed homologue to monkey area 12[79,80]), the frontal eye field (or around it), and the precentral ventral frontal gyrus.

Functional properties of the distributed cortical networks associated with the human MTL

Classical neurophysiological models of human memory were inspired by animal anatomical studies suggesting that the hippocampus is located at the apex of cortical hierarchy[81] and receives highly integrated unimodal, polymodal, and supramodal cortical input, which allows it to form abstract and rich mnemonic representations that characterize declarative memory.[82] Our data show that the cortical pathways associated with the human MTL integrate information coming from at least three different distributed cortical networks spanning human association cortex. The pathway associated with the human parahippocampal area TH corresponds to one subdivision of the default network, labeled as default network A.[53,54] This subdivision has been recently shown to be selectively engaged during episodic simulation of past and future events, and during spatial processing.[55,71,83] The pathway associated with the human entorhinal cortex corresponds to another subdivision of the default network, labeled as default network B.[53,54] This subdivision has been shown to be specifically engaged during social processing that involves imagining perspective of other agents.[55,84–86] The pathway associated with the human perirhinal cortex corresponds to the subdivision A of the dorsal attention network[69,87,88] that is typically engaged during visuospatial externally oriented tasks. While the exact functional specialization of the different subdivisions of the dorsal attention network is unknown, our data provide initial evidence that the subdivision A is associated with the MTL and that at least parts of the subdivision B are not associated with the MTL. It has been shown that the dorsal attention network has stronger functional coupling with unimodal visual and motor regions compared with other distributed brain networks.[67] Because of the topographical proximity between different visual areas in humans, it was speculated that visual sensory information might propagate from early visual areas to MT+ and then to the area anterior to MT+, which we find to be associated with the perirhinal cortex.[67,81,89] Therefore, we speculate that the subdivision A of the dorsal attention network is a source of visual input to the human MTL by way of the perirhinal cortex and potentially parahippocampal area TF.

Exploratory analyses

Even though our observations regarding the connectivity patterns of the human pre/parasubiculum with the broader neocortex and the differential connectivity patterns of the dorsal vs. ventral posterior collateral sulcus are of exploratory nature, they nevertheless pave way for exciting future research. Our exploratory observations regarding the pre/parasubiculum connectivity are consistent with monkey observations showing that areas comprising the subicular complex are anatomically connected with multiple cortical brain regions, including the inferior parietal lobe, retrosplenial cortex, and frontal cortex.[16,18,90] Given that direct anatomical connections between the hippocampus proper and the neocortex (excluding the MTL) are minute,[91] this is a crucial anatomical pathway, as it directly connects the broader neocortex with the hippocampal formation bypassing the parahippocampal, perirhinal, and entorhinal cortices (see also Barnett et al.[39]). Our additional exploratory observations about the differential connectivity profiles within the posterior collateral sulcus align with the parcellation of the parahippocampal cortex into the medially situated area TH and laterally situated area TF. Originally, von Economo and Koskinas[13] suggested that area TH spans the entire parahippocampal gyrus and the lateral bank of the collateral sulcus, whereas area TF extends laterally all the way through the fusiform gyrus. In later cytoarchitectonic studies, von Bonin and Bailey[14,92] used the same TH/TF nomenclature, but argued that area TF is located more medially and it does not extend beyond the lateral bank of the collateral sulcus. Recent human studies suggest that area TF is mostly buried within the walls of the collateral sulcus or occupies

only its lateral bank. Therefore, localization of human parahippocampal areas TH/TF is ambiguous.[48,49] Nevertheless, our exploratory findings suggest that human parahippocampal cortex potentially comprises at least two distinct subregions characterized by different connectivity with the broader neocortex. These fine anatomical dissociations are striking, and they emphasize the importance of precision neuroimaging approaches as leverage for discovery.

Insights from comparisons to monkey anatomy

Comparison between our findings and monkey anatomy suggests three novel insights. First insight is that multiple anatomical connections of the memory system are preserved across human and non-human primates. This mostly pertains to the anatomical connections of the broader neocortex with parahippocampal area TH. Except for the connections with the unimodal auditory and visual areas, the parahippocampal pathways involving the posterior parietal cortex, dorsolateral and medial frontal cortex, posteromedial cortex, and some minute connections to the lateral temporal cortex are clearly preserved in humans. Other preserved anatomical pathways are the connections between the entorhinal cortex and the temporal pole/lateral temporal cortex, posteromedial cortex, and medial frontal cortex. The perirhinal cortex also shows some anatomical cross-species preservation that pertains to the ventrolateral frontal cortex and potentially to the superior parietal lobe.

The second insight is that our data suggest that the human MTL is only minimally associated with unimodal sensory processing (Figure S3; see also Figure S6B for more analyses and discussion). In monkey, the MTL is a nexus of sensory convergence that receives directly unimodal association inputs from high-order auditory, visual, and somatosensory cortices. In humans, however, our results suggest that input to the MTL is dominated by brain areas that are not involved in unimodal sensory processing.[40]

The third and perhaps the most exciting insight is that we provide evidence for potentially novel cortical pathways in the human memory system compared with non-human primates. In particular, this pertains to the pathways involving the entorhinal cortex. In monkeys, the entorhinal cortex is connected with both the posterior cingulate and retrosplenial cortices, whereas in our human data, the entorhinal cortex showed preferred connectivity to the posterior cingulate cortex over the most ventral parts of the posteromedial cortex. Furthermore, monkey data indicate only faint anatomical connectivity between the caudal entorhinal cortex and the inferior parietal cortex.[76,93] On the other hand, our human data suggest strong associations between the human entorhinal cortex and the inferior parietal lobule (however, it is unclear if this is a newly developed area or a subdivision of monkey area 7a). Finally, while monkey anatomical studies indicate only light connections between the entorhinal cortex and the dorsolateral frontal cortex, we show that these connections are more pronounced in humans. These differences suggest that either a novel cortical network emerged in humans or an existing network in monkeys was functionally specialized in humans[71] (also see Whitesell et al.[94]). Since the network associated with the human entorhinal cortex has suggested to be selectively engaged in social processing,[55,71] we speculate that this is an evolutionary recent network that could develop following the extensive cortical expansion in humans.[95]

Limitations

Our study has two major limitations. The first limitation pertains to anatomical interpretability of fMRI connectivity methods. Even though correlations in intrinsic brain activity patterns were proved to be a powerful means for studying anatomical connectivity, one must keep in mind that MRI functional connectivity methods are a *proxy* for mono- and polysynaptic anatomical connectivity. Therefore, when comparing human connectivity observations with known animal anatomy, interpretation of negative results is challenging—"new" connections observed in humans can in principle result from polysynaptic connectivity. Furthermore, absence of functional connectivity between brain regions cannot indicate lack of anatomical connectivity. It is also important to consider that many animal tract-tracing experiments contain "hidden" data, either unpublished or not looked for. Therefore, no evidence for anatomical connectivity between certain regions does not mean that this connectivity does not exist.

The second limitation of our study relates to the divisions of the different subregions of the MTL. The entorhinal, perirhinal, and parahippocampal cortices are not homogeneous, and each of them can be divided into distinct subdivisions. Traditionally, the entorhinal cortex has been considered to comprise at least two subdivisions—lateral and medial entorhinal cortex. This subdivision is particularly accepted in the rodent, where the two subdivisions can be easily differentiated using cytoarchitectonic analysis and patterns of anatomical projections.[96,97] In primates, no clear cytoarchitectonically defined division of the entorhinal cortex into lateral and medial subdivisions exists[98], and it was suggested that the primate homologues of the rodent lateral and medial entorhinal cortex are located in the anterior and posterior entorhinal cortex, respectively.[99] Given the size of the human entorhinal cortex, our voxel size, spatial smoothing parameters, gross anatomical location, and whole-brain connectivity patterns, we are highly likely to sample from a few entorhinal divisions, which we believe represent the posterior subdivisions of the entorhinal cortex.[98] Even though previous fMRI connectivity studies point to differential connectivity patterns within subregions of the human entorhinal cortex,[42,47,100] in our datasets, we could not consistently identify distinct seeds within the most anterior portion of the entorhinal cortex that were associated with biologically meaningful whole-brain network topography (Figure S7A and Video S5). The perirhinal cortex can also be divided into area BA35 (medially situated and mostly buried within the rhinal sulcus in the monkey) and larger area BA36 (more laterally situated[101]). While animal tract-tracing studies indicate differential connectivity of these perirhinal divisions with the broader neocortex,[20] we could not identify distinct connectivity patterns from sampling the medial and the lateral walls of the anterior part of the collateral sulcus (see Videos S1 and S2). In fact, the location of perirhinal areas BA35 and BA36 along the collateral sulcus depends on the depth of the sulcus. In some cases, when the collateral sulcus is extremely shallow (see Figure 2F in Insausti et al.[51]), the

perirhinal area BA36 extends over the fusiform gyrus, and then area BA35 occupies the lateral bank of the sulcus. Even though in our study the perirhinal seeds were positioned closer to the lateral bank of the collateral sulcus, most likely sampling from area BA36, it is still a possibility that area BA35 was sampled instead. The parahippocampal cortex can also be divided at least into areas TH and TF. In our current study, we believe that our parahippocampal seeds specifically target parahippocampal area TH, and we provide initial evidence for a dissociation between areas TH/TF. For pursuing further these questions of fine grain anatomical subdivisions of the entorhinal, perirhinal, and parahippocampal cortices, further neuroimaging research focused on within-subject analysis is required.

Conclusions

Using precision neuroimaging focused on individuals, our findings significantly extend previous group-level reports by providing a robust estimation of at least three distributed cortical networks linked to the human memory system. The evolutionary insights gained from comparing our observations to known monkey anatomy highlights the importance of comparative neuroanatomy approach in studying the developmental trajectory of mnemonic functions.

STAR★METHODS

Detailed methods are provided in the online version of this paper and include the following:

- KEY RESOURCES TABLE
- RESOURCE AVAILABILITY
  - Lead contact
  - Materials availability
  - Data and code availability
- EXPERIMENTAL MODEL AND STUDY PARTICIPANT DETAILS
  - Human participants
- METHOD DETAILS
  - MRI data acquisition
  - Phase encoding direction
  - Data processing
  - Data quality and susceptibility artifacts
  - Networks discovery
  - Networks validation
  - Replication analyses using different MTL seeds
  - Consistency of MTL connectivity maps
  - Subdivisions of the dorsal attention network
  - Cortical networks associated with the temporal pole
  - Connectivity between subregions of the human MTL
  - Replication using UK Biobank fixation task data
- QUANTIFICATION AND STATISTICAL ANALYSIS

SUPPLEMENTAL INFORMATION

Supplemental information can be found online at https://doi.org/10.1016/j.neuron.2023.05.029.

ACKNOWLEDGMENTS

D.R. thanks Randy L. Buckner, Jared Nielsen, Rodrigo M. Braga, and Lauren M. DiNicola for inspiring conversations about within-subject functional connectivity and neuroanatomy. The authors thank Domenica Klank, Kerrin Pine, Lea-Sofie Funk, Kerstin Schumer, and Heidrun Schultz for their help with data acquisition and administrative support. The authors thank Martin Hebart, Sofie Valk, Falk Eippert, Misun Kim, and Simone Viganó for helpful comments. Davide Chiarugi and Markus Then assisted with data processing. This work is supported by the Max Planck Society. C.F.D.'s research is further supported by the European Research Council (ERC-CoG GEOCOG 724836), the Kavli Foundation, the Jebsen Foundation, Helse Midt-Norge, and The Research Council of Norway (223262/F50; 197467/F50). N.W. has received funding from the European Union's Horizon 2020 research and innovation program under the grant agreement No 681094, from the Deutsche Forschungsgemeinschaft (DFG, German Research Foundation) under project no. 347592254 (WE 5046/4-2), and from the Federal Ministry of Education and Research (BMBF) under support code 01ED2210.

AUTHOR CONTRIBUTIONS

D.R. and C.F.D. designed the study, D.R. and R.T. collected the data, D.R. analyzed the data with input from C.F.D., M.P.W. provided critical anatomical input, D.R. wrote the original draft, D.R., R.T., N.W., M.P.W., and C.F.D. edited and wrote the manuscript; C.F.D. secured funding.

DECLARATION OF INTERESTS

The Max Planck Institute for Human Cognitive Sciences has an institutional research agreement with Siemens Healthcare. N.W. holds a patent on acquisition of MRI data during spoiler gradients (US 10,401,453 B2). N.W. was a speaker at an event organized by Siemens Healthcare and was reimbursed for the travel expenses.

INCLUSION AND DIVERSITY

We support inclusive, diverse, and equitable conduct of research.

Received: November 25, 2022
Revised: May 26, 2023
Accepted: May 27, 2023
Published: June 29, 2023

REFERENCES

1. Alvarez, P., and Squire, L.R. (1994). Memory consolidation and the medial temporal lobe: A simple network model. Proc. Natl. Acad. Sci. USA *91*, 7041–7045. https://doi.org/10.1073/pnas.91.15.7041.
2. Eichenbaum, H., Yonelinas, A.P., and Ranganath, C. (2007). The medial temporal lobe and recognition memory. Annu. Rev. Neurosci. *30*, 123–152. https://doi.org/10.1146/annurev.neuro.30.051606.094328.
3. Milner, B., Corkin, S., and Teuber, H.L. (1968). Further analysis of the hippocampal amnesic syndrome: 14-year follow-up study of H. M. Neuropsychologia *6*, 215–234. https://doi.org/10.1016/0028-3932(68)90021-3.
4. Mishkin, M. (1978). Memory in monkeys severely impaired by combined but not by separate removal of amygdala and hippocampus. Nature *273*, 297–298. https://doi.org/10.1038/273297a0.
5. Scoville, W.B., and Milner, B. (1957). Loss of recent memory after bilateral hippocampal lesions. J. Neurol. Neurosurg. Psychiatry *20*, 11–21. https://doi.org/10.1136/jnnp.20.1.11.
6. Squire, L.R., and Zola-Morgan, S. (1991). The medial temporal lobe memory system. Science *253*, 1380–1386. https://doi.org/10.1126/science.1896849.
7. Amaral, D.G., and Witter, M.P. (1989). The three-dimensional organization of the hippocampal formation: A review of anatomical data.

Neuroscience *31*, 571–591. https://doi.org/10.1016/0306-4522(89)90424-7.

8. Lavenex, P., and Amaral, D.G. (2000). Hippocampal-neocortical interaction: A hierarchy of associativity. Hippocampus *10*, 420–430. https://doi.org/10.1002/1098-1063(2000)10:4<420::AID-HIPO8>3.0.CO;2-5.
9. Ranganath, C., and Ritchey, M. (2012). Two cortical systems for memory-guided behaviour. Nat. Rev. Neurosci. *13*, 713–726. https://doi.org/10.1038/nrn3338.
10. Ritchey, M., Libby, L.A., and Ranganath, C. (2015). Cortico-hippocampal systems involved in memory and cognition: The PMAT framework. Prog. Brain Res. *219*, 45–64. https://doi.org/10.1016/bs.pbr.2015.04.001.
11. Agster, K.L., and Burwell, R.D. (2009). Cortical efferents of the perirhinal, postrhinal, and entorhinal cortices of the rat. Hippocampus *19*, 1159–1186. https://doi.org/10.1002/hipo.20578.
12. Burwell, R.D., and Amaral, D.G. (1998). Cortical afferents of the perirhinal, postrhinal, and entorhinal cortices of the rat. J. Comp. Neurol. *398*, 179–205. https://doi.org/10.1002/(SICI)1096-9861(19980824)398:2<179::AID-CNE3>3.0.CO;2-Y.
13. von Economo, C., and Koskinas, G. (1925). Die Cytoarchitecktonik der Grosshirnrinde des erwachsenen Menschen (Springer).
14. von Bonin, G., and Bailey, P. (1947). The Neocortex of Macaca mulatta (University of Illinois Press).
15. Pandya, D.N., and Seltzer, B. (1982). Intrinsic connections and architectonics of posterior parietal cortex in the rhesus monkey. J. Comp. Neurol. *204*, 196–210. https://doi.org/10.1002/cne.902040208.
16. Cavada, C., and Goldman-Rakic, P.S. (1989). Posterior parietal cortex in rhesus monkey: II. Evidence for segregated corticocortical networks linking sensory and limbic areas with the frontal lobe. J. Comp. Neurol. *287*, 422–445. https://doi.org/10.1002/cne.902870403.
17. Distler, C., Boussaoud, D., Desimone, R., and Ungerleider, L.G. (1993). Cortical connections of inferior temporal area TEO in macaque monkeys. J. Comp. Neurol. *334*, 125–150. https://doi.org/10.1002/cne.903340111.
18. Kobayashi, Y., and Amaral, D.G. (2003). Macaque monkey retrosplenial cortex: II. Cortical afferents. J. Comp. Neurol. *466*, 48–79. https://doi.org/10.1002/cne.10883.
19. Lavenex, P., Suzuki, W.A., and Amaral, D.G. (2002). Perirhinal and parahippocampal cortices of the macaque monkey: Projections to the neocortex. J. Comp. Neurol. *447*, 394–420. https://doi.org/10.1002/cne.10243.
20. Suzuki, W.A., and Amaral, D.G. (1994). Perirhinal and parahippocampal cortices of the macaque monkey: Cortical afferents. J. Comp. Neurol. *350*, 497–533. https://doi.org/10.1002/cne.903500402.
21. Amaral, D.G., Insausti, R., and Cowan, W.M. (1983). Evidence for a direct projection from the superior temporal gyrus to the entorhinal cortex in the monkey. Brain Res. *275*, 263–277. https://doi.org/10.1016/0006-8993(83)90987-3.
22. Goldman-Rakic, P.S., Selemon, L.D., and Schwartz, M.L. (1984). Dual pathways connecting the dorsolateral prefrontal cortex with the hippocampal formation and parahippocampal cortex in the rhesus monkey. Neuroscience *12*, 719–743. https://doi.org/10.1016/0306-4522(84)90166-0.
23. Insausti, R., Amaral, D.G., and Cowan, W.M. (1987). The entorhinal cortex of the monkey: II. Cortical afferents. J. Comp. Neurol. *264*, 356–395. https://doi.org/10.1002/cne.902640306.
24. Disotell, T.R., and Tosi, A.J. (2007). The monkey's perspective. Genome Biol. *8*, 226. https://doi.org/10.1186/gb-2007-8-9-226.
25. Gallant, J.L., Shoup, R.E., and Mazer, J.A. (2000). A human extrastriate area functionally homologous to macaque V4. Neuron *27*, 227–235. https://doi.org/10.1016/S0896-6273(00)00032-5.
26. Öngür, D., Ferry, A.T., and Price, J.L. (2003). Architectonic subdivision of the human orbital and medial prefrontal cortex. J. Comp. Neurol. *460*, 425–449. https://doi.org/10.1002/cne.10609.
27. Petrides, M., Tomaiuolo, F., Yeterian, E.H., and Pandya, D.N. (2012). The prefrontal cortex: Comparative architectonic organization in the human and the macaque monkey brains. Cortex *48*, 46–57. https://doi.org/10.1016/j.cortex.2011.07.002.
28. Chaplin, T.A., Yu, H.H., Soares, J.G.M., Gattass, R., and Rosa, M.G.P. (2013). A conserved pattern of differential expansion of cortical areas in simian primates. J. Neurosci. *33*, 15120–15125. https://doi.org/10.1523/JNEUROSCI.2909-13.2013.
29. Hill, J., Inder, T., Neil, J., Dierker, D., Harwell, J., and Van Essen, D. (2010). Similar patterns of cortical expansion during human development and evolution. Proc. Natl. Acad. Sci. USA *107*, 13135–13140. https://doi.org/10.1073/pnas.1001229107.
30. Van Essen, D.C., and Dierker, D.L. (2007). Surface-based and probabilistic atlases of primate cerebral cortex. Neuron *56*, 209–225. https://doi.org/10.1016/j.neuron.2007.10.015.
31. Kenet, T., Bibitchkov, D., Tsodyks, M., Grinvald, A., and Arieli, A. (2003). Spontaneously emerging cortical representations of visual attributes. Nature *425*, 954–956. https://doi.org/10.1038/nature02078.
32. Biswal, B., Yetkin, F.Z., Haughton, V.M., and Hyde, J.S. (1995). Functional connectivity in the motor cortex of resting human brain using echo-planar mri. Magn. Reson. Med. *34*, 537–541. https://doi.org/10.1002/mrm.1910340409.
33. Fox, M.D., Snyder, A.Z., Vincent, J.L., Corbetta, M., Van Essen, D.C., and Raichle, M.E. (2005). The human brain is intrinsically organized into dynamic, anticorrelated functional networks. Proc. Natl. Acad. Sci. USA *102*, 9673–9678. https://doi.org/10.1073/pnas.0504136102.
34. Krienen, F.M., and Buckner, R.L. (2009). Segregated fronto-cerebellar circuits revealed by intrinsic functional connectivity. Cereb. Cortex. *19*, 2485–2497. https://doi.org/10.1093/cercor/bhp135.
35. Tavor, I., Parker Jones, O., Mars, R.B., Smith, S.M., Behrens, T.E., and Jbabdi, S. (2016). Task-free MRI predicts individual differences in brain activity during task performance. Science *352*, 216–220. https://doi.org/10.1126/science.aad8127.
36. Vincent, J.L., Kahn, I., Van Essen, D.C., and Buckner, R.L. (2010). Functional connectivity of the macaque posterior parahippocampal cortex. J. Neurophysiol. *103*, 793–800. https://doi.org/10.1152/jn.00546.2009.
37. Vincent, J.L., Patel, G.H., Fox, M.D., Snyder, A.Z., Baker, J.T., Van Essen, D.C., Zempel, J.M., Snyder, L.H., Corbetta, M., and Raichle, M.E. (2007). Intrinsic functional architecture in the anaesthetized monkey brain. Nature *447*, 83–86. https://doi.org/10.1038/nature05758.
38. Liu, C., Yen, C.C.C., Szczupak, D., Ye, F.Q., Leopold, D.A., and Silva, A.C. (2019). Anatomical and functional investigation of the marmoset default mode network. Nat. Commun. *10*, 1975. https://doi.org/10.1038/s41467-019-09813-7.
39. Barnett, A.J., Reilly, W., Dimsdale-Zucker, H.R., Mizrak, E., Reagh, Z., and Ranganath, C. (2021). Intrinsic connectivity reveals functionally distinct cortico-hippocampal networks in the human brain. PLoS Biol. *19*, e3001275. https://doi.org/10.1371/journal.pbio.3001275.
40. Kahn, I., Andrews-Hanna, J.R., Vincent, J.L., Snyder, A.Z., and Buckner, R.L. (2008). Distinct cortical anatomy linked to subregions of the medial temporal lobe revealed by intrinsic functional connectivity. J. Neurophysiol. *100*, 129–139. https://doi.org/10.1152/jn.00077.2008.
41. Libby, L.A., Ekstrom, A.D., Ragland, J.D., and Ranganath, C. (2012). Differential connectivity of perirhinal and parahippocampal cortices within human hippocampal subregions revealed by high-resolution functional imaging. J. Neurosci. *32*, 6550–6560. https://doi.org/10.1523/JNEUROSCI.3711-11.2012.
42. Navarro-Schröder, T., Haak, K.V., Jimenez, N.I.Z., Beckmann, C.F., and Doeller, C.F. (2015). Functional topography of the human entorhinal cortex. Elife *4*, e06738. https://doi.org/10.7554/eLife.06738.
43. Qin, S., Duan, X., Supekar, K., Chen, H., Chen, T., and Menon, V. (2016). Large-scale intrinsic functional network organization along the long axis

of the human medial temporal lobe. Brain Struct. Funct. *221*, 3237–3258. https://doi.org/10.1007/s00429-015-1098-4.

44. Ruiz-Rizzo, A.L., Beissner, F., Finke, K., Müller, H.J., Zimmer, C., Pasquini, L., and Sorg, C. (2020). Human subsystems of medial temporal lobes extend locally to amygdala nuclei and globally to an allostatic-interoceptive system. Neuroimage *207*, 116404. https://doi.org/10.1016/j.neuroimage.2019.116404.
45. Seoane, S., Modroño, C., González-Mora, J.L., and Janssen, N. (2022). Medial temporal lobe contributions to resting-state networks. Brain Struct. Funct. *227*, 995–1012. https://doi.org/10.1007/s00429-021-02442-1.
46. Wang, S.F., Ritchey, M., Libby, L.A., and Ranganath, C. (2016). Functional connectivity based parcellation of the human medial temporal lobe. Neurobiol. Learn. Mem. *134*, 123–134. https://doi.org/10.1016/j.nlm.2016.01.005.
47. Maass, A., Berron, D., Libby, L.A., Ranganath, C., and Düzel, E. (2015). Functional subregions of the human entorhinal cortex. Elife *4*, e06426. https://doi.org/10.7554/eLife.06426.
48. Insausti, R., Insausti, A.M., Sobreviela, M.T., Salinas, A., and Martínez-Peñuela, J.M. (1998). Human medial temporal lobe in aging: Anatomical basis of memory preservation. Microsc. Res. Tech. *43*, 8–15. https://doi.org/10.1002/(SICI)1097-0029(19981001)43:1<8::AID-JEMT2>3.0.CO;2-4.
49. Thangavel, R., Van Hoesen, G.W., and Zaheer, A. (2008). Posterior parahippocampal gyrus pathology in Alzheimer's disease. Neuroscience *154*, 667–676. https://doi.org/10.1016/j.neuroscience.2008.03.077.
50. Webster, M.J., Ungerleider, L.G., and Bachevalier, J. (1991). Connections of inferior temporal areas TE and TEO with medial temporal-lobe structures in infant and adult monkeys. J. Neurosci. *11*, 1095–1116. https://doi.org/10.1523/jneurosci.11-04-01095.1991.
51. Insausti, R., Juottonen, K., Soininen, H., Insausti, A.M., Partanen, K., Vainio, P., Laakso, M.P., and Pitkänen, A. (1998). MR volumetric analysis of the human entorhinal, perirhinal, and temporopolar cortices. AJNR. Am. J. Neuroradiol. *19*, 659–671.
52. Krimer, L.S., Hyde, T.M., Herman, M.M., and Saunders, R.C. (1997). The entorhinal cortex: An examination of cyto- and myeloarchitectonic organization in humans. Cereb. Cortex *7*, 722–731. https://doi.org/10.1093/cercor/7.8.722.
53. Braga, R.M., Van Dijk, K.R.A., Polimeni, J.R., Eldaief, M.C., and Buckner, R.L. (2019). Parallel distributed networks resolved at high resolution reveal close juxtaposition of distinct regions. J. Neurophysiol. *121*, 1513–1534. https://doi.org/10.1152/jn.00808.2018.
54. Braga, R.M., and Buckner, R.L. (2017). Parallel Interdigitated Distributed Networks within the Individual Estimated by Intrinsic Functional Connectivity. Neuron *95*, 457–471.e5. https://doi.org/10.1016/j.neuron.2017.06.038.
55. DiNicola, L.M., Braga, R.M., and Buckner, R.L. (2020). Parallel distributed networks dissociate episodic and social functions within the individual. J. Neurophysiol. *123*, 1144–1179. https://doi.org/10.1152/jn.00529.2019.
56. Ortega, M., Hoyt-Drazen, C., Gratton, C., Newbold, D.J., Greene, D.J., Berg, J.J., Gordon, E.M., Laumann, T.O., Gilmore, A.W., Sun, H., et al. (2017). Precision Functional Mapping of Individual Human NeuroResource Precision Functional Mapping of Individual Human Brains. Neuron *95*, 791–807.e7.
57. Gordon, E.M., Laumann, T.O., Gilmore, A.W., Newbold, D.J., Greene, D.J., Berg, J.J., Ortega, M., Hoyt-Drazen, C., Gratton, C., Sun, H., et al. (2017). Precision Functional Mapping of Individual Human Brains. Neuron *95*, 791–807.e7. https://doi.org/10.1016/j.neuron.2017.07.011.
58. Gordon, E.M., Laumann, T.O., Adeyemo, B., and Petersen, S.E. (2017). Individual Variability of the System-Level Organization of the Human Brain. Cereb. Cortex *27*, 386–399. https://doi.org/10.1093/cercor/bhv239.
59. Marek, S., Siegel, J.S., Gordon, E.M., Raut, R.V., Gratton, C., Newbold, D.J., Ortega, M., Laumann, T.O., Adeyemo, B., Miller, D.B., et al. (2018). Spatial and Temporal Organization of the Individual Human Cerebellum. Neuron *100*, 977–993.e7. https://doi.org/10.1016/j.neuron.2018.10.010.
60. Xue, A., Kong, R., Yang, Q., Eldaief, M.C., Angeli, P.A., DiNicola, L.M., Braga, R.M., Buckner, R.L., and Yeo, B.T.T. (2021). The detailed organization of the human cerebellum estimated by intrinsic functional connectivity within the individual. J. Neurophysiol. *125*, 358–384. https://doi.org/10.1152/jn.00561.2020.
61. Krienen, F.M., Yeo, B.T.T., and Buckner, R.L. (2014). Reconfigurable task-dependent functional coupling modes cluster around a core functional architecture. Philos. Trans. R. Soc. Lond. B Biol. Sci. *369*, 20130526. https://doi.org/10.1098/rstb.2013.0526.
62. Finn, E.S. (2021). Is it time to put rest to rest? Trends Cogn. Sci. *25*, 1021–1032. https://doi.org/10.1016/j.tics.2021.09.005.
63. Chen, X., Vieweg, P., and Wolbers, T. (2019). Computing distance information from landmarks and self-motion cues - Differential contributions of anterior-lateral vs. posterior-medial entorhinal cortex in humans. Neuroimage *202*, 116074. https://doi.org/10.1016/j.neuroimage.2019.116074.
64. Berron, D., Cardenas-Blanco, A., Bittner, D., Metzger, C.D., Spottke, A., Heneka, M.T., Fliessbach, K., Schneider, A., Teipel, S.J., Wagner, M., et al. (2019). Higher CSF tau levels are related to hippocampal hyperactivity and object mnemonic discrimination in older adults. J. Neurosci. *39*, 8788–8797. https://doi.org/10.1523/JNEUROSCI.1279-19.2019.
65. Koster, R., Chadwick, M.J., Chen, Y., Berron, D., Banino, A., Düzel, E., Hassabis, D., and Kumaran, D. (2018). Big-Loop Recurrence within the Hippocampal System Supports Integration of Information across Episodes. Neuron *99*, 1342–1354.e6. https://doi.org/10.1016/j.neuron.2018.08.009.
66. Chadwick, M.J., Jolly, A.E.J., Amos, D.P., Hassabis, D., and Spiers, H.J. (2015). A goal direction signal in the human entorhinal/subicular region. Curr. Biol. *25*, 87–92. https://doi.org/10.1016/j.cub.2014.11.001.
67. Yeo, B.T.T., Krienen, F.M., Sepulcre, J., Sabuncu, M.R., Lashkari, D., Hollinshead, M., Roffman, J.L., Smoller, J.W., Zöllei, L., Polimeni, J.R., et al. (2011). The organization of the human cerebral cortex estimated by intrinsic functional connectivity. J. Neurophysiol. *106*, 1125–1165. https://doi.org/10.1152/jn.00338.2011.
68. Yarkoni, T., Poldrack, R.A., Nichols, T.E., Van Essen, D.C., and Wager, T.D. (2011). Large-scale automated synthesis of human functional neuroimaging data. Nat. Methods *8*, 665–670. https://doi.org/10.1038/nmeth.1635.
69. Corbetta, M., Patel, G., and Shulman, G.L. (2008). The Reorienting System of the Human Brain: From Environment to Theory of Mind. Neuron *58*, 306–324. https://doi.org/10.1016/j.neuron.2008.04.017.
70. Huntgeburth, S.C., and Petrides, M. (2012). Morphological patterns of the collateral sulcus in the human brain. Eur. J. Neurosci. *35*, 1295–1311. https://doi.org/10.1111/j.1460-9568.2012.08031.x.
71. Buckner, R.L., and DiNicola, L.M. (2019). The brain's default network: updated anatomy, physiology and evolving insights. Nat. Rev. Neurosci. *20*, 593–608. https://doi.org/10.1038/s41583-019-0212-7.
72. Kobayashi, Y., and Amaral, D.G. (2007). Macaque monkey retrosplenial cortex: III. Cortical efferents. J. Comp. Neurol. *502*, 810–833. https://doi.org/10.1002/cne.21346.
73. Suzuki, W.A., and Amaral, D.G. (2003). Perirhinal and parahippocampal cortices of the Macaque monkey: Cytoarchitectonic and chemoarchitectonic organization. J. Comp. Neurol. *463*, 67–91. https://doi.org/10.1002/cne.10744.
74. Seltzer, B., and Pandya, D.N. (1984). Further observations on parieto-temporal connections in the rhesus monkey. Exp. Brain Res. *55*, 301–312. https://doi.org/10.1007/BF00237280.
75. Ding, S.L., Van Hoesen, G., and Rockland, K.S. (2000). Inferior parietal lobule projections to the presubiculum and neighboring ventromedial

temporal cortical areas. J. Comp. Neurol. *425*, 510–530. https://doi.org/10.1002/1096-9861(20001002)425:4<510::AID-CNE4>3.0.CO;2-R.

76. Muñoz, M., and Insausti, R. (2005). Cortical efferents of the entorhinal cortex and the adjacent parahippocampal region in the monkey (Macaca fascicularis). Eur. J. Neurosci. *22*, 1368–1388. https://doi.org/10.1111/j.1460-9568.2005.04299.x.
77. Cavada, C., and Goldman-Rakic, P.S. (1989). Posterior parietal cortex in rhesus monkey: I. Parcellation of areas based on distinctive limbic and sensory corticocortical connections. J. Comp. Neurol. *287*, 393–421. https://doi.org/10.1002/cne.902870402.
78. Van Essen, D.C. (2003). Organization of Visual Areas in Macaque and Human Cerebral Cortex. The Visual Neurosciences *2*, 507–521. https://doi.org/10.7551/mitpress/7131.003.0038.
79. Petrides, M., and Pandya, D.N. (1999). Dorsolateral prefrontal cortex: Comparative cytoarchitectonic analysis"in the human and the macaque brain and corticocortical connection patterns. Eur. J. Neurosci. *11*, 1011–1036. https://doi.org/10.1046/j.1460-9568.1999.00518.x.
80. Petrides, M. (2005). Lateral prefrontal cortex: Architectonic and functional organization. Philos. Trans. R. Soc. Lond. B Biol. Sci. *360*, 781–795. https://doi.org/10.1098/rstb.2005.1631.
81. Felleman, D.J., and Van Essen, D.C. (1991). Distributed hierarchical processing in the primate cerebral cortex. Cereb. Cortex *1*, 1–47. https://doi.org/10.1093/cercor/1.1.1.
82. Squire, L.R. (1992). Declarative and nondeclarative memory: Multiple brain systems supporting learning and memory. J. Cogn. Neurosci. *4*, 232–243. https://doi.org/10.1162/jocn.1992.4.3.232.
83. Hartley, T., Maguire, E.A., Spiers, H.J., and Burgess, N. (2003). The well-worn route and the path less traveled: Distinct neural bases of route following and wayfinding in humans. Neuron *37*, 877–888. https://doi.org/10.1016/S0896-6273(03)00095-3.
84. Andrews-Hanna, J.R., Saxe, R., and Yarkoni, T. (2014). Contributions of episodic retrieval and mentalizing to autobiographical thought: Evidence from functional neuroimaging, resting-state connectivity, and fMRI meta-analyses. Neuroimage *91*, 324–335. https://doi.org/10.1016/j.neuroimage.2014.01.032.
85. Saxe, R., and Kanwisher, N. (2003). People thinking about thinking people: The role of the temporo-parietal junction in "theory of mind. Neuroimage *19*, 1835–1842. https://doi.org/10.1016/S1053-8119(03)00230-1.
86. Saxe, R., and Wexler, A. (2005). Making sense of another mind: The role of the right temporo-parietal junction. Neuropsychologia *43*, 1391–1399. https://doi.org/10.1016/j.neuropsychologia.2005.02.013.
87. Fox, M.D., Corbetta, M., Snyder, A.Z., Vincent, J.L., and Raichle, M.E. (2006). Spontaneous neuronal activity distinguishes human dorsal and ventral attention systems. Proc. Natl. Acad. Sci. USA *103*, 10046–10051. https://doi.org/10.1073/pnas.0604187103.
88. Petersen, S.E., and Posner, M.I. (2012). The attention system of the human brain: 20 years after. Annu. Rev. Neurosci. *35*, 73–89. https://doi.org/10.1146/annurev-neuro-062111-150525.
89. Maunsell, J., and Van Essen, D.C. (1983). The Connections of the Middel Temporal Visual Area (MT) and Their Relationship to a Cortical Hie. J. Neurosci. *3*, 2563–2586.
90. Rosene, D.L., and Van Hoesen, G.W. (1977). Hippocampal efferents reach widespread areas of cerebral cortex and amygdala in the rhesus monkey. Science *198*, 315–317. https://doi.org/10.1126/science.410102.
91. Insausti, R., and Muñoz, M. (2001). Cortical projections of the non-entorhinal hippocampal formation in the cynomolgus monkey (Macaca fascicularis). Eur. J. Neurosci. *14*, 435–451. https://doi.org/10.1046/j.0953-816X.2001.01662.x.
92. Bailey, P., and von Bonin, G. (1951). The Isocortex of Man (University of Illinois Press).
93. Mohedano-Moriano, A., Pro-Sistiaga, P., Arroyo-Jimenez, M.M., Artacho-Pérula, E., Insausti, A.M., Marcos, P., Cebada-Sánchez, S., Martínez-Ruiz, J., Muñoz, M., Blaizot, X., et al. (2007). Topographical and laminar distribution of cortical input to the monkey entorhinal cortex. J. Anatomy *211*, 250–260. https://doi.org/10.1111/j.1469-7580.2007.00764.x.
94. Whitesell, J.D., Liska, A., Coletta, L., Hirokawa, K.E., Bohn, P., Williford, A., Groblewski, P.A., Graddis, N., Kuan, L., Knox, J.E., et al. (2021). Regional, Layer, and Cell-Type-Specific Connectivity of the Mouse Default Mode Network. Neuron *109*, 545–559.e8. https://doi.org/10.1016/j.neuron.2020.11.011.
95. Saxe, R. (2006). Uniquely human social cognition. Curr. Opin. Neurobiol. *16*, 235–239. https://doi.org/10.1016/j.conb.2006.03.001.
96. Witter, M.P. (2007). The perforant path: projections from the entorhinal cortex to the dentate gyrus. Prog. Brain Res. *163*, 43–61. https://doi.org/10.1016/S0079-6123(07)63003-9.
97. Kjonigsen, L.J., Leergaard, T.B., Witter, M.P., and Bjaalie, J.G. (2011). Digital atlas of anatomical subdivisions and boundaries of the rat hippocampal region. Front. Neuroinform. *5*, 2. https://doi.org/10.3389/fninf.2011.00002.
98. Insausti, R., Belichenko, P.V., Frotscher, M., Matus, A., Monyer, H., Palm, G., and Steinhäuser, C. (1993). Comparative anatomy of the entorhinal cortex and hippocampus in mammals. Hippocampus *3*, 289–292. https://doi.org/10.1002/hipo.1993.4500030705.
99. Witter, M.P., and Amaral, D.G. (2021). The entorhinal cortex of the monkey: VI. Organization of projections from the hippocampus, subiculum, presubiculum, and parasubiculum. J. Comp. Neurol. *529*, 828–852. https://doi.org/10.1002/cne.24983.
100. Syversen, I.F., Witter, M.P., Kobro-Flatmoen, A., Goa, P.E., Navarro Schröder, T., and Doeller, C.F. (2021). Structural connectivity-based segmentation of the human entorhinal cortex. Neuroimage *245*, 118723. https://doi.org/10.1016/j.neuroimage.2021.118723.
101. Suzuki, W.A., and Amaral, D.G. (2003). Where are the perirhinal and parahippocampal cortices? A historical overview of the nomenclature and boundaries applied to the primate medial temporal lobe. Neuroscience *120*, 893–906. https://doi.org/10.1016/S0306-4522(03)00281-1.
102. Cox, R.W. (2012). AFNI: What a long strange trip it's been. Neuroimage *62*, 743–747. https://doi.org/10.1016/j.neuroimage.2011.08.056.
103. Marcus, D.S., Harwell, J., Olsen, T., Hodge, M., Glasser, M.F., Prior, F., Jenkinson, M., Laumann, T., Curtiss, S.W., and Van Essen, D.C. (2011). Informatics and data mining tools and strategies for the human connectome project. Front. Neuroinform. *5*, 4. https://doi.org/10.3389/fninf.2011.00004.
104. Fischl, B. (2012). Neuroimage *62*, 774–781. https://doi.org/10.1016/j.neuroimage.2012.01.021.
105. Smith, S.M., Jenkinson, M., Woolrich, M.W., Beckmann, C.F., Behrens, T.E.J., Johansen-Berg, H., Bannister, P.R., De Luca, M., Drobnjak, I., Flitney, D.E., et al. (2004). Advances in functional and structural MR image analysis and implementation as FSL. Neuroimage *23*, S208–S219. https://doi.org/10.1016/j.neuroimage.2004.07.051.
106. Majka, P., Chaplin, T.A., Yu, H.H., Tolpygo, A., Mitra, P.P., Wójcik, D.K., and Rosa, M.G.P. (2016). Towards a comprehensive atlas of cortical connections in a primate brain: Mapping tracer injection studies of the common marmoset into a reference digital template. J. Comp. Neurol. *524*, 2161–2181. https://doi.org/10.1002/cne.24023.
107. Majka, P., Bai, S., Bakola, S., Bednarek, S., Chan, J.M., Jermakow, N., Passarelli, L., Reser, D.H., Theodoni, P., Worthy, K.H., et al. (2020). Open access resource for cellular-resolution analyses of corticocortical connectivity in the marmoset monkey. Nat. Commun. *11*, 1133. https://doi.org/10.1038/s41467-020-14858-0.
108. Miller, K.L., Alfaro-Almagro, F., Bangerter, N.K., Thomas, D.L., Yacoub, E., Xu, J., Bartsch, A.J., Jbabdi, S., Sotiropoulos, S.N., Andersson, J.L.R., et al. (2016). Multimodal population brain imaging in the UK

Biobank prospective epidemiological study. Nat. Neurosci. *19*, 1523–1536. https://doi.org/10.1038/nn.4393.

109. Reznik, D., DiNicola, L.M., Braga, R.M., Angeli, P., and Buckner, R.L. (2019). Cortical networks associated with the human anterior medial temporal lobe estimated within the individual using intrinsic functional connectivity. In Program number 427.17. 2019 *Neuroscience meeting planner* (Society for Neuroscience).

110. Greve, D.N., and Fischl, B. (2009). Accurate and robust brain image alignment using boundary-based registration. Neuroimage *48*, 63–72. https://doi.org/10.1016/j.neuroimage.2009.06.060.

111. Cox, R.W. (1996). AFNI: Software for analysis and visualization of functional magnetic resonance neuroimages. Comput. Biomed. Res. *29*, 162–173. https://doi.org/10.1006/cbmr.1996.0014.

112. Fischl, B., Sereno, M.I., Tootell, R.B.H., and Dale, A.M. (1999). High-resolution intersubject averaging and a coordinate system for the cortical surface. Hum. Brain Mapp. *8*, 272–284. https://doi.org/10.1002/(SICI)1097-0193(1999)8:4<272::AID-HBM10>3.0.CO;2-4.

113. van Dijk, K.R.A., Sabuncu, M.R., and Buckner, R.L. (2012). The influence of head motion on intrinsic functional connectivity MRI. Neuroimage *59*, 431–438. https://doi.org/10.1016/j.neuroimage.2011.07.044.

114. Du, J., and Buckner, R.L. (2021). Precision estimates of macroscale network organization in the human and their relation to anatomical connectivity in the marmoset monkey. Curr. Opin. Behav. Sci. *40*, 144–152. https://doi.org/10.1016/j.cobeha.2021.04.010.

115. Duvernoy, H. (1999). The Human Brain: Surface, Three-Dimensional Sectional Anatomy with MRI, and Blood Supply (Springer Science & Business Media).

116. Vincent, J.L., Kahn, I., Snyder, A.Z., Raichle, M.E., and Buckner, R.L. (2008). Evidence for a frontoparietal control system revealed by intrinsic functional connectivity. J. Neurophysiol. *100*, 3328–3342. https://doi.org/10.1152/jn.90355.2008.

117. Insausti, R. (2013). Comparative neuroanatomical parcellation of the human and nonhuman primate temporal pole. J. Comp. Neurol. *521*, 4163–4176. https://doi.org/10.1002/cne.23431.

118. Pascual, B., Masdeu, J.C., Hollenbeck, M., Makris, N., Insausti, R., Ding, S.L., and Dickerson, B.C. (2015). Large-scale brain networks of the human left temporal pole: A functional connectivity MRI study. Cereb. Cortex. *25*, 680–702. https://doi.org/10.1093/cercor/bht260.

119. Doan, T.P., Lagartos-Donate, M.J., Nilssen, E.S., Ohara, S., and Witter, M.P. (2019). Convergent Projections from Perirhinal and Postrhinal Cortices Suggest a Multisensory Nature of Lateral, but Not Medial, Entorhinal Cortex. Cell Rep. *29*, 617–627.e7. https://doi.org/10.1016/j.celrep.2019.09.005.

120. Lavenex, P., Suzuki, W.A., and Amaral, D.G. (2004). Perirhinal and Parahippocampal Cortices of the Macaque Monkey: Intrinsic Projections and Interconnections. J. Comp. Neurol. *472*, 371–394. https://doi.org/10.1002/cne.20079.

121. Gordon, E.M., Chauvin, R.J., Van, A.N., Rajesh, A., Nielsen, A., Newbold, D.J., Lynch, C.J., Seider, N.A., Krimmel, S.R., Scheidter, K.M., et al. (2023). A somato-cognitive action network alternates with effector regions in motor cortex. Nature *617*, 351–359. https://doi.org/10.1038/s41586-023-05964-2.

STAR★METHODS

KEY RESOURCES TABLE

REAGENT or RESOURCE	SOURCE	IDENTIFIER
Software and algorithms		
AFNI	Cox, 2012[102]	https://afni.nimh.nih.gov/
Connectome Workbench	Marcus et al., 2011[103]	http://www.humanconnectome.org/software/connectome-workbench
FreeSurfer	Fischl, 201[104]	https://surfer.nmr.mgh.harvard.edu/
FSL	Smith et al., 2004[105]	https://fsl.fmrib.ox.ac.uk/fsl/fslwiki
Marmoset tracing data	Majka et al., 2016, 2020[106,107]	https://www.marmosetbrain.org/
MATLAB	Mathworks	https://www.mathworks.com/
MATLAB code for Connectome Workbench		https://github.com/Washington-University/cifti-matlab
UK Biobank data and documentation	Miller et al., 2016[108]	https://www.fmrib.ox.ac.uk/ukbiobank/ https://biobank.ctsu.ox.ac.uk/crystal/ukb/docs/brain_mri.pdf

RESOURCE AVAILABILITY

Lead contact

Further information and requests for resources should be directed to and will be fulfilled by the lead contact, Daniel Reznik (reznik@cbs.mpg.de or reznikda@gmail.com).

Materials availability

This study did not generate new unique reagents.

Data and code availability

- De-identified data that supports the findings of this study are available via Mendeley Data in the following link - https://doi.org/10.17632/jzxz3xkws6.1.
- This paper does not report original code.
- Any additional information required to reanalyse the data reported in this paper is available from the lead contact upon request.

EXPERIMENTAL MODEL AND STUDY PARTICIPANT DETAILS

Human participants

Four healthy human participants (2 females and 2 males; 20, 26, 31, and 32 years old) were recruited for this study from the participants database of the Max Planck Institute for Human Cognitive and Brains Science, Leipzig, Germany. The sample size was based on previous precision neuroimaging work estimating functional connectivity within individual.[53,54,60,109] The study involved 4 separate MRI scanning sessions comprising only fixation tasks ("resting state" data), and the participants were rewarded with an additional monetary payment for completing all 4 sessions. All participants provided written consent in accordance with guidelines approved by the ethics committee of Leipzig University.

METHOD DETAILS

MRI data acquisition

MR data were collected on a 7T Siemens MAGNETOM Terra scanner with pTX capability (Siemens Healthineers, Erlangen, Germany) equipped with whole-body gradients (70 mT/m maximum amplitude and 200 T/m/s maximum slew rate). An 8-channel transmit/32-channel receive coil (Nova Medical, Wilmington MA, USA) was used for radio frequency transmission and reception. We decided to use a 7T scanner since it allows to collect fMRI data with higher SNR at high spatial resolutions compared with 3T scanners. Moreover, BOLD sensitivity is greater and it peaks at an earlier echo time (TE) at 7T compared to 3T. To leverage this advantage of 7T, we used a TE of 18 milliseconds, which would be too short for optimal BOLD contrast at 3T. Such an unusually short TE allowed us to

collect whole brain 7T data with relatively high temporal resolution of 1500 milliseconds, which resulted in more temporal data-points necessary for robust intrinsic functional connectivity analysis.

Each of the 4 scanning sessions consisted of 8 fixation tasks ("resting state"), each lasting 7 mins and 28 seconds, for estimating intrinsic functional connectivity. Functional imaging data were acquired using a 2D, multi-band gradient-echo echo-planar imaging (EPI) pulse sequence with the following parameters: repetition time (TR) = 1500ms; TE = 18ms; flip angle 60°; isotropic spatial resolution of 1.5mm; field of view of 192 × 192 × 120mm^3; 80 interleaved slices covering the entire cerebral cortex and the cerebellum without gaps; GRAPPA factor of 3; multiband factor of 2. The EPI sequence was a custom sequence provided by the Center for Magnetic Resonance Research (CMRR) at University of Minnesota (Moeller et al., 2010; Setsompop et al., 2012); sequence parameters were piloted and optimized for highest image quality.

To estimate the distortions caused by static magnetic field (B_0) inhomogeneities, the phase-encoding polarity technique was applied which combines two spin-echo EPI scans with different phase encoding directions (anterior-posterior and posterior-anterior). The field map was estimated from the difference in distortion between the two acquisitions. Field of view, imaging matrix, slice thickness and bandwidth for the Spin-Echo EPI scans were identical to the fMRI acquisition parameters. For the spin-echo scans, we used a TR of 7 s (dictated by SAR restrictions) and a TE of 41 ms. Fixation tasks were interleaved with Spin Echo EPI scans in a way that each resulting field map was used for unwarping the two temporally adjacent task runs (Figure 1). During one of the scanning sessions, a T1-weighted structural image was acquired using an MP2RAGE three-dimensional sequence with TR = 5000 ms; TE = 2.17 ms; spatial resolution of 1mm isotropic; inversion times (TI)1/2 = 900/2750 ms; flip angles (FA)1/2 = 5/3°; band width = 200 Hz/Px; phase partial Fourier = 6/8.

During the fixation task runs, participants were instructed to remain still, stay awake and to focus on a white crosshair presented in a center of a black screen. During the Spin Echo EPI scans, participants were allowed to close their eyes, but were instructed not to fall asleep. To reduce head movement, participants were encouraged to find the most comfortable lying position prior to scanning. We did not use an objective measure to monitor our participants' drowsiness level during scanning, such as an eye camera. However, our analysis of the movement artifacts indicated minimal head displacement for all participants (except for one session, out of total 128, that was excluded), which can serve as an indirect indication that participants remained alert throughout the scanning procedure. The scanner room lights were kept dim and participants were talked to after each task and Spin-Echo EPI scans to ensure they are ready to continue and whether they would like a break.

Phase encoding direction

Previous functional connectivity fMRI studies showed that the anterior portion of the MTL is linked to areas around the temporal pole.[40,41] Therefore, during acquisition of the fMRI data using the typical anterior-posterior phase encoding direction, it is possible that data from this anterior region will be geometrically projected to adjacent posteriorly situated brain regions, including the entorhinal and perirhinal cortex. Therefore, with BOLD data acquired using the anterior-posterior phase encoding direction, seeds located in the anterior MTL might actually sample non-MTL fMRI signals. Even though we used field maps to correct for geometrical distortions occurring during data acquisition and to reconstruct the original anatomy, to avoid as much as possible projection of BOLD signal from anterior portions of the temporal lobe and other anteriorly located regions to the anterior portion of the MTL, all fixation tasks data were acquired with a posterior-anterior phase encoding direction.

Data processing

Processing of the fMRI data was optimized for within-subject analysis to preserve anatomical detail across different scanning sessions. Each participant was processed separately, and data handling followed closely the steps described in detail in Braga et al.[53] Overall, five spatial transformation matrixes were calculated for each available BOLD run:

Matrix 1 – motion correction – each available BOLD run was motion corrected by aligning all volumes within a run to its middle volume. The alignment was performed with a linear registration (FSL v6.0.1[105]).

Matrix 2 – field map correction – every middle volume from all available BOLD runs was field map unwarped using the session-specific and run-specific field map. We used not only session-specific, but also run-specific (i.e., within sessions) field maps as participants' head position in the scanner typically changes throughout the scanning session (even with minimal within-run head movement), thus introducing run-specific inhomogeneities which we aimed to account for. Field maps were prepared using FSL *topup* (FSL v6.0.1[105]).

Matrix 3 – alignment to the mean BOLD template – field map unwrapped middle volumes from each run were then registered to a participant-specific mean BOLD template which was created in 2 steps. First, we took the field map unwrapped middle volume of the BOLD run that was acquired closest to the T1-weighted structural image and linearly registered to it all field map unwrapped middle volumes from all available runs. Then, we averaged all these aligned middle volumes to create a participant specific mean BOLD template to which all field map unwrapped middle volumes were linearly registered with 12 DOF (FSL, v6.0.1[105]). By averaging all the aligned middle volumes in creating the mean BOLD template, we wanted to minimize any bias toward any one run or session.

Matrix 4 – alignment to T1 space – the mean BOLD template was then registered to the T1 native space using boundary-based registration implemented in FREESURFER (v7.0.1[104,110]).

Matrix 5 – alignment to MNI space – we then projected the data from T1 space to MNI space using nonlinear registration in FSL (v6.0.1[105]).

Matrices 1–5 were combined into a single interpolation transformation that was then applied to the original raw volumes from all available BOLD runs. We used this single interpolation (as opposed to serial interpolations of the data applied step-after-step) to reduce interpolation artifacts and to maintain as much as possible anatomical detail of within-participant datasets. Matrices 1–4 were combined in a similar way to project the data to T1 native space.

To prepare the data for functional connectivity analysis, nuisance variables (six motion parameters, whole brain signal, ventricular signal, and white matter signal) and their temporal derivatives (computed by backward differences) were derived from BOLD data projected to the native T1 space. All signals were regressed out of both T1-and MNI-space data using *3dTproject* (AFNI v19.1.05[102,111]). This was followed by bandpass filtering at 0.01–0.1 Hz using *3dBandpass* (AFNI v19.1.05[102,111]). MNI-space volumetric data were then spatially smoothed (FSL v6.0.1[105]). Initially, all participants' data were smoothed using a 4 mm full width at half-maximum (FWHM) kernel. During a preliminary connectivity analysis (excluding and prior to MTL exploration), participants 2 and 4 showed more blurred cortical networks (which can be partly seen in the unthresholded maps presented in Figure S3), therefore these participants' data were smoothed using a 3 mm FWHM kernel (see also Braga et al.[53] for applying different smoothing kernels to different participants; Figure S3B shows MTL connectivity maps from participants 2 and 4 smoothed with a 4 mm FWHM kernel).

For visualization purposes, the MNI-space connectivity maps that were created in the volumentric data, were projected to T1 space and resampled to the fsaverage6 standardized cortical surface mesh (40,962 vertices per hemisphere[112]). For the cortical surface projection, data were sampled from the gray matter halfway between the white matter and pial surfaces using trilinear interpolation. Surface maps were visualized using the Connectome Workbench command *wb_view*.[103] For this purpose, fsaverage6 surface-projected data were converted into CIFTI format using Workbench MATLAB commands (v2022a; https://github.com/Washington-University/cifti-matlab).

Data quality and susceptibility artifacts

Head motion is known to affect functional connectivity and to drive spurious correlation patterns (for example, see Figure 4 in Van Dijk et al.[113]). To minimize the effect of head motion on our connectivity findings, every BOLD run with maximum absolute head displacement greater than 2 mm was discarded from the analysis. Additionally, imaging the brain regions in the anterior MTL is a longstanding challenge since these regions are particularly prone to signal loss and distortion due to magnetic inhomogeneities seen clearly in T_2*-weighted images (BOLD data). To estimate the overall data quality, we calculated tSNR in every voxel by averaging the signal intensity in all available BOLD runs (prior to nuisance variables regression, filtering and smoothing) for each participant and dividing it by the standard deviation over time. The tSNR maps were averaged separately for each participant to provide a single tSNR value for each voxel in the brain.

Networks discovery

Following the logic described in Braga & Buckner,[54] to reliably test for different cortical networks associated with distinct subregions of the human MTL, for each participant we divided all available BOLD data into discovery and validation datasets. After 4 scanning sessions with 8 fixations tasks each, every participant had up to 32 BOLD runs (~230 min). All odd-numbered runs were assigned to a discovery dataset (16 fixations task runs) and all even-numbered runs were assigned to a validation dataset (16 fixations task runs). We excluded one fixation task run for participant 4 due to extensive head motion (see data quality in results), therefore, the validation dataset for that participant comprised 15 fixations task runs. All connectivity analyses were done on volumetric data in MNI-space since we wanted to use a common reference frame which allows comparison of our findings with other studies.

Human MTL is immensely variable and its anatomy strongly depends on the sulcal pattern. Therefore, we adopted a seed-based method for network discovery and validation rather than a group-level mask-based analysis to examine each participant's data in depth and to move away from MTL-related group-based priors. The hypotheses for our connectivity study were biologically driven from primate tract-tracing work showing that macaque entorhinal, perirhinal and parahippocampal cortices are anatomically connected with multiple distributed brain regions, such as posterior middle, parietal lobe, frontal lobe, temporal lobe and visual cortex. We aimed to use human MR precision neuroimaging as a discovery tool to resolve a fundamental question in human memory research and to identify the distributed cortical areas associated with the cortical components of the human MTL. Our study did not seek to confirm expectations from previous human group-level connectivity studies dealing with whole-brain MTL connectivity (especially, with the anterior MTL). In our data, we expected that subregions of the human MTL will show distributed connectivity patterns that can broadly resemble the distributed connectivity patterns observed in macaque data. We used human group-level and individual-level cortical distributed networks as a general reference; these findings are highly robust and most importantly, they have a strong biological basis, such that many of these networks can be identified also in the primate.[114]

One critical aspect of our analysis approach was using only half of the data for exploring the MTL and for generating hypotheses about potentially different networks associated with its subregions. Therefore, all seed regions and hypothesized networks were defined using *only* the discovery datasets (half of the data). Then, in the hypothesis-testing step (see below), we used independent datasets (other half of the data) to either provide support or reject the hypotheses that distinct subregions of the human MTL are associated with different cortical networks.

For the discovery analysis, for each participant we explored in detail the anterior-posterior and the medial-lateral axes of the parahippocampal gyrus and the collateral sulcus. Seed regions were single voxels selected from the gray matter and positioned on the mean BOLD image in MNI space. We used macroanatomical landmarks for determining the approximate location of the entorhinal,

perirhinal and parahippocampal cortices.[48,51,115] On the anterior-posterior axis, the most anterior segment of the parahippocampal gyrus (containing the suspected entorhinal cortex) was determined as the first slice with visible amygdala.[51] The most posterior segment of the parahippocampal gyrus (containing the suspected parahippocampal areas TH/TF) was determined as the last slice with visible hippocampus. On the medial-lateral axis, the most medial point was positioned ventrally to the subicular complex. The most lateral point was positioned in the ventral part of the lateral bank of collateral sulcus (see Videos S1, S2, S3, S4, and S5 for examples of seed placement showcasing raw data). Anatomical landmarks were identified in each participant using an anatomical atlas containing human brain photos, the corresponding structural MR images and detailed anatomical labels at different slices.[115]

For each examined MTL seed, we calculated whole-brain Pearson correlation coefficients between the seed voxel's time series and all other voxels' time series for every discovery BOLD run using *instacorr* (AFNI v19.1.05[102,111]). Resulting Pearson correlation coefficients were Fisher z-transformed and averaged across all discovery dataset BOLD runs. Functional connectivity maps for every seed voxel were visually inspected and if they showed a set of distributed brain regions that strongly correlated with the seed voxel, the seed voxel was used for further analysis. Strong correlations with the distributed brain regions were defined as $z(r) > 0.3$ for the seeds in the anterior segment of the MTL, containing the candidate entorhinal and perirhinal cortices and $z(r) > 0.5$ for the seeds in the posterior segment of the MTL, containing the candidate parahippocampal cortex. For participant 3, that showed overall weaker correlations, strong correlations with seeds in the anterior segment of the MTL were defined as $z(r) > 0.2$. Negative correlation values were not interpreted. Since we performed the discovery analysis in the volume space, correlations in the white matter and ventricles, as well as low gray matter correlations of $z(r) < 0.15$ were considered spurious (see Figure S7A for an example of spurious correlations). To determine the level of spurious correlations, we placed large spherical seeds within the deep white matter (5mm radius) and the ventricles (2mm radius), and calculated whole-brain Fisher z-transformed Pearson correlation coefficients. The 99-th percentile of positive correlations ($z(r) = 0.15$) was taken as the noise correlation threshold (see also Braga et al.[53] for using a similar threshold for a volume-based within-subject intrinsic functional connectivity analysis). We visualize the process of seed placement in Videos S1 and S2 (anterior MTL) and Videos S3 and S4 (posterior MTL); all examples display raw unthresholded data. For instance, as can be seen from Videos S1 and S2, moving the seed along the parahippocampal gyrus and the collateral sulcus in the anterior segments of the MTL produced two clear hypotheses for two distributed networks associated with distinct regions of the parahippocampal gyrus and the collateral sulcus. These hypothesized networks were present in each individual participant's anterior MTL. As can be seen from Videos S3 and S4, moving the seed along the parahippocampal gyrus and the collateral sulcus in the posterior segment of the MTL resulted in one clear hypothesis of another distributed cortical network (note clear evidence for mixture of signals with moving the seed along the collateral sulcus, possibly due to smoothing of BOLD data from the banks of the sulcus; as the results unfolded, this mixture of signals was resolved as potential parahippocampal areas TH/TF; see results and discussion; see Video S5 for movement of the seed along the anterior-posterior axis of the parahippocampal gyrus). These hypotheses were then blindly tested using independent validation datasets (see below).

Following the discovery analysis, for each participant we identified a set of seed voxels located in different portions of the parahippocampal gyrus and collateral sulcus that strongly correlated with distinct set of distributed brain regions. For each participant, these voxels occupied continues segments on the anterior-posterior and medial-lateral axes of the parahippocampal gyrus and collateral sulcus, albeit in different locations. Across all participants, one set of seed voxels was located in the anterior medial portion of the parahippocampal gyrus, medially to the collateral sulcus, anatomically corresponding to the entorhinal cortex and more specifically, to its posterior medial part. Another set of seed voxels was located in the lateral bank of the anterior portion of the collateral sulcus, anatomically corresponding to the perirhinal cortex (the suspected perirhinal seeds were always more anteriorly or just around the suspected entorhinal seeds, corresponding to the relative anatomical locations of these MTL regions[51]). Another set of seed voxels was located in the posterior medial portion of the parahippocampal gyrus (anatomically corresponding to the potential parahippocampal area TH). These voxels were identified by visualizing the connectivity maps at a threshold of $z(r) > 0.15$ (above the noise correlation level) and by inspecting the anatomical locations of different cortical areas that consistently correlated with subregions of the MTL across all participants—posterior midline, anterior midline, parietal lobe, lateral frontal cortex and lateral surface of the temporal lobe (as can be seen in Figure S3, even unthresholded connectivity maps showed little overlap in all 4 participants). It is important to emphasize that even though we explored the MTL for seeds that maximize potential networks separation, these seeds and their associated distributed brain regions represented only *hypotheses* for distinct networks linked to different parts of the MTL. Therefore, a critical step was to put these hypotheses to an independent test and to examine whether distinct associations of the MTL seeds with different areas across the cortical mantle will be replicated using independent validation datasets.

Connectivity patterns that were not consistently present in each individual participant were not tested during the hypothesis-validation step. In our data we observed two potentially meaningful inconsistent connectivity patterns. First, participant 4 showed a candidate network (however with much weaker correlations compared to other candidate networks) associated with the most ventral tip of the entorhinal cortex (Figure S7C). The distributed whole-brain topography associated with this region bore some resemblance to components of the frontoparietal control network.[116] Even though this connectivity pattern is remarkably compliant with known primate anatomy[106,107,114] (appreciate the marmoset tracing results presented in Figure S7C demonstrating labeled cells just at the border between the entorhinal and perirhinal cortices, similar to our seed location), since no other participant provided clear evidence for this association, it was not further pursued. Second, some participants showed distinct connectivity patterns with seeds positioned in the medial and lateral portions of the suspected parahippocampal cortex, occupying the medial and lateral banks of the

collateral sulcus. However, this connectivity pattern was not consistent as well across all participants. As the results unfolded, this was resolved as potential parahippocampal areas TH/TF (see results and discussion).

Networks validation

After identifying the distinct sets of seed voxels that maximized potential networks separation using the discovery datasets, one seed with the highest or near to highest Fisher z-transformed Pearson correlation coefficient with the distributed brain regions was taken as the representative seed for each MTL region – posterior entorhinal cortex, perirhinal cortex and parahippocampal area TH (see below replication analyses using multiple different MTL seeds). For the hypotheses-testing step using the independent validation datasets, for each chosen MTL seed and for each participant, we identified the voxels with maximum Fisher z-transformed Pearson correlation values in the parietal lobe, dorsolateral frontal cortex, posteromedial cortex, and ventral medial prefrontal cortex. The voxels were always identified in the hemisphere ipsilateral to each given MTL seed. This seeds definition was done using *only* the discovery datasets. We choose these cortical dissociation regions for independent validation purposes as either two or all three subregions of the MTL showed strong, however close, correlations in these areas. Since the validation datasets were analyzed blindly of the discovery datasets, the critical test was to see whether the *a priori* chosen seed regions in the MTL and the cortical dissociation regions will replicate the connectivity patterns observed during the discovery analysis. Specifically, we wanted to see whether the distinct seeds in the parietal lobe, dorsolateral frontal cortex, posteromedial cortex, and ventral medial prefrontal cortex will show distinct "back-projection" connectivity to the subregions of the MTL. For testing the hypothesis that distinct MTL regions are associated with distinct brain regions, the connectivity patterns derived from the validation datasets were statistically tested using F-tests with one-way or two-way repeated measures analysis of variance (ANOVA). One-way ANOVA was used in each MTL subregion for testing the dissociation regions that showed correlations with all three subregions of the MTL (parietal lobe, dorsolateral frontal cortex). Two-way ANOVA was used for testing the dissociation regions that showed correlations with two subregions of the MTL (posteromedial cortex, ventral medial prefrontal cortex).

Replication analyses using different MTL seeds

To demonstrate that our results do not depend on one particular seed selection, we choose different seeds by moving the original seeds 6 mm toward each other (3 mm shift for each seed separately) on the anterior-posterior axis. Therefore, the suspected entorhinal and perirhinal seeds were shifted caudally toward the parahippocampal cortex and the suspected parahippocampal seeds were shifted rostrally toward the entorhinal and perirhinal cortex. The decision to shift the seeds exactly 6 mm toward each other was semi-arbitrary. Moving the seeds only 2 mm toward each other would be too close to the original seed location and the replication would be obvious. However, moving the seeds 10 mm toward each other would be too big of a shift and the suspected entorhinal and perirhinal seeds would then likely sample signal from the parahippocampal cortex. Therefore, the middle ground of 6 mm shift was chosen. Even with these new seeds that were optimally pitted against each other, we replicate all our findings reported in Figure 4, except for a preferred correlation of the perirhinal seed with the dorsolateral frontal cortex in participant 1. Moreover, like in the original results, all participants showed cross-over interaction effects where relevant. Furthermore, we examined how our results generalize in the anterior direction as well. We shifted all original entorhinal seeds 3 mm rostrally and performed the same analyses. All effects reported in Figure 4 were replicated. We also shifted the perirhinal seeds 3 mm rostrally for participant 1 and participant 3 (in participant 2 and participant 4 the original perirhinal seeds were already positioned very rostrally) and performed the same analyses. All effect reported in Figure 4 were replicated. Finally, we shifted all original parahippocampal seeds 0.5 cm rostrally to move them even closer toward the entorhinal and perirhinal cortices. All effects presented in Figure 4 were replicated except for a preferred entorhinal seed connectivity with the parietal lobe and dorsolateral frontal cortex in participant 4 due to potential blurring and mixture of signals across networks.

Consistency of MTL connectivity maps

To examine the consistency of whole brain functional connectivity maps from each MTL subregion, we correlated the mean functional connectivity matrices from the discovery and replication datasets in each participant. Connectivity maps showed high stability across discovery and validation datasets with minimum Pearson correlation coefficient of 0.81 (all $p < 0.001$) across participants and MTL subregions.

Subdivisions of the dorsal attention network

The two subdivisions A and B of the canonical dorsal attention network can be robustly dissociated from each other by the collateral sulcus (potentially involving the fusiform gyrus and the lingual gyrus; see Figures 23 and 25 in Yeo, Krienen et al.,[67] and bottom of Figure 5 in Braga & Buckner[54]). Using the discovery datasets, we put spherical seeds of 3 mm radius in the middle of the occipital collateral sulcus (anatomically defined[70,115]) in each participant. The middle of the occipital collateral sulcus was determined as the middle *y* coordinate between the last slice with visible hippocampus and the last slice with visible occipital cortex. The seed was always positioned within the sulcus to avoid sampling signal from the white matter and to allow sampling from the surrounding fusiform and lingual gyri. See Figure 7A for the cortical projection of the distributed brain regions associated with the occipital collateral sulcus (right column; putative subdivision B) and the "back-projections" from the superior parietal lobule associated with the perirhinal cortex (left column; putative subdivision B). Next, still using the discovery datasets, we identified in each participant the voxels

with maximum Fisher z-transformed Pearson correlation coefficients in the superior parietal lobe and in the suspected MT+. We aimed to localize these cortical regions as the perirhinal network showed strong correlations located in their vicinity. Then, using validation datasets, we performed similar "back-projection" analyses to see whether the connectivity patterns of the neighboring seeds in the superior parietal lobule and the extrastriate cortex (area anterior to MT+ and MT+) with the perirhinal cortex and the occipital collateral sulcus will be replicated (see results and Figure 7B).

Cortical networks associated with the temporal pole

The study by Wang et al.[46] examined the cortical anatomy associated with the anterior perirhinal cortex and observed perirhinal-auditory associations. Based on this observation, the authors raised an intriguing possibility that the anterior segment of the human perirhinal cortex is a homologue of monkey area 36d. In our investigation of the human MTL, we found no consistent auditory associations with the human MTL. Nevertheless, we wished to explore the cortical networks associated with the human temporal polar cortex[117] as the putative human homologue of the rostral extension of the monkey perirhinal cortex area 36. Even though this rostral area is a direct continuation of the perirhinal cortex, in the macaque, the connectivity patterns of at least a part of the polar cortex with the broader neocortex and cytoarchitectonic characteristics are different from the rest of the perirhinal cortex. Therefore, it is still unclear whether the temporal polar cortex should be regarded as a subdivision of the perirhinal cortex.[73,101] In our data, seeds put directly into the temporal pole[118] produced connectivity maps resembling the entorhinal network (Figure S7B). Since the observed connectivity patterns were not compliant with the reported anatomical connectivity of the monkey area 36d, we do not discuss this finding any further and leave this to future investigations.

Connectivity between subregions of the human MTL

Our results show low correlations between the entorhinal, perirhinal and parahippocampal seeds (Table S1). At first glance, this observation does not comply with animal neuroanatomy studies showing anatomical connectivity between the entorhinal, perirhinal and parahippocampal (postrhinal in the rodent) cortices. However, a more detailed look into our seed locations and tract-tracing rodent and primate data can potentially account for this observation.

First, recent anatomical data in the rodent suggest that both postrhinal and perirhinal cortices predominantly target the lateral entorhinal cortex[119]; re-evaluation of anatomical MTL data from the macaque suggests similar connectivity patterns. These findings challenge the classical cognitive models for differential sensory ("what", mediated by the perirhinal-lateral entorhinal cortex connectivity) and spatial ("where", mediated by the parahippocampal-medial entorhinal cortex connectivity) processing within the entorhinal cortex[2,9] and highlight the lateral entorhinal cortex as the main multimodal convergence area in the parahippocampal region. These findings can potentially account for our results, since the proposed primate homologue of the lateral entorhinal cortex is situated in the anterior portion of the entorhinal cortex,[99] while our entorhinal seeds are likely located in the posterior entorhinal cortex. Like we mention in the main text, previous human group-level studies were able to delineate potential subdivisions of the entorhinal cortex,[42,47,100] however, in our datasets focused on individuals, we could not identify distinct seeds within the most anterior portion of the entorhinal cortex that were associated with biologically meaningful signal (Figure S7A and Video S5). Therefore, one key question for future MTL precision imaging is to reliably characterize the distributed anatomy associated with the most anterior portion of human entorhinal cortex.

Second, tract-tracing in the macaque indicates that the vast majority of anatomical connections between the perirhinal and parahippocampal cortices involve parahippocampal area TF, while the perirhinal cortex connections with parahippocampal area TH are much more modest.[120] These observations are compliant with our findings showing low connectivity between parahippocampal area TH and the perirhinal cortex (Table S1), and that parahippocampal area TF and the perirhinal cortex are associated with similar cortical anatomy (Figure 8).

Replication using UK Biobank fixation task data

Inspired by Gordon et al.,[121] we used the publicly available voxel-wise whole-brain connectome computed on 4100 participants[108] from the initial release of the UK-Biobank fMRI dataset (see https://biobank.ctsu.ox.ac.uk/crystal/ukb/docs/brain_mri.pdf for documentation). Using anatomical heuristics, we put seeds in the putative entorhinal, perirhinal, and parahippocampal cortices and calculated whole-brain connectivity maps. The resulting maps were projected to the surface and thresholded to display only correlations greater than 2 standard deviations from the mean (for the perirhinal seed, the threshold was 1.5 standard deviations from the mean). The resulting maps are presented in Figure S8B. These population-level results provide additional evidence supporting our individual-level observations associating different subregions of the human MTL with distinct cortical networks.

QUANTIFICATION AND STATISTICAL ANALYSIS

In this study, 4 participants were scanned 4 times each, which resulted in 32 fixation task ("resting-state") runs for each individual participant. Half of the data (16 runs) were assigned to the discovery datasets and the other half of the data (16 runs) were assigned to the validation datasets. For participant 4 one run was excluded due to excessive head movement (2.9 mm), therefore, the validation dataset for this participant comprised 15 runs. Functional connectivity analysis was performed separately in each participant using AFNI *instacorr* command which allowed interactive exploration of the whole-brain connectivity patterns in each

participant.[102,111] Resulting Pearson correlation coefficients were Fisher z-transformed and averaged across all discovery datasets BOLD runs. Localization of different anatomical landmarks was done using an anatomical atlas as refence containing human brain photos, the corresponding structural MR images and detailed anatomical labels at different slices.[115] For statistical analyses we used one-way and two-way repeated measures ANOVA with significance level set to $p < 0.05$. All bar graphs throughout the manuscript represent mean Fisher z-transformed Pearson correlation coefficients ± SEM.

Neuron, Volume *111*

Supplemental information

Dissociating distinct cortical networks associated with subregions of the human medial temporal lobe using precision neuroimaging

Daniel Reznik, Robert Trampel, Nikolaus Weiskopf, Menno P. Witter, and Christian F. Doeller

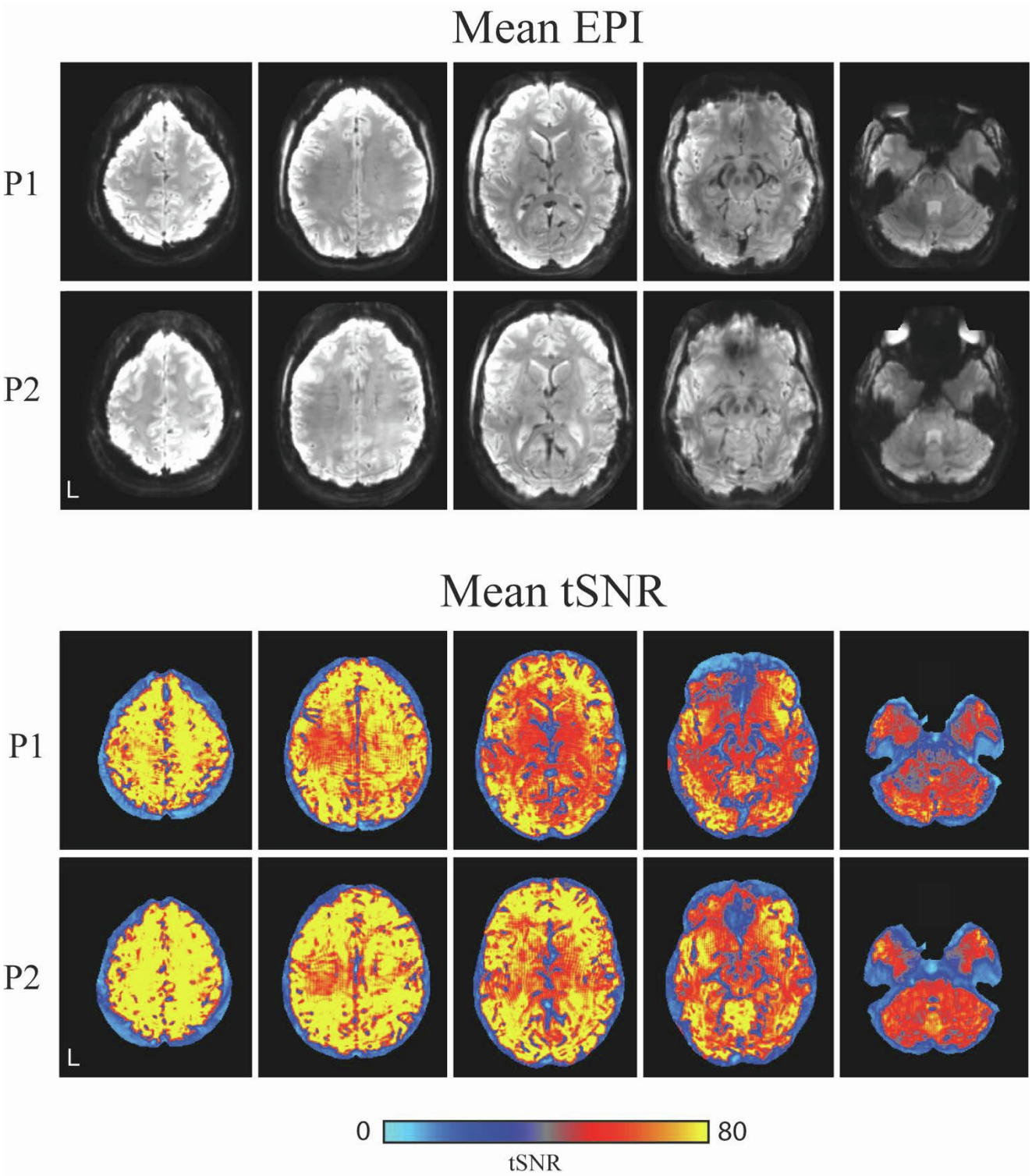

Figure S1. Data quality. Related to Figure 1 in the main text. Axial slices from participants 1 and 2 (P1, P2) showing mean BOLD (*top*) and mean tSNR (*bottom*) data. High coverage and high tSNR were obtained in most regions of the brain, particularly in the medial temporal lobe. Note lower data quality in the ventral portions of the medial prefrontal cortex and the lateral surface of the temporal lobes. See Figure 1 for the same data from participants 3 and 4. Left on the image (L) refers to left hemisphere.

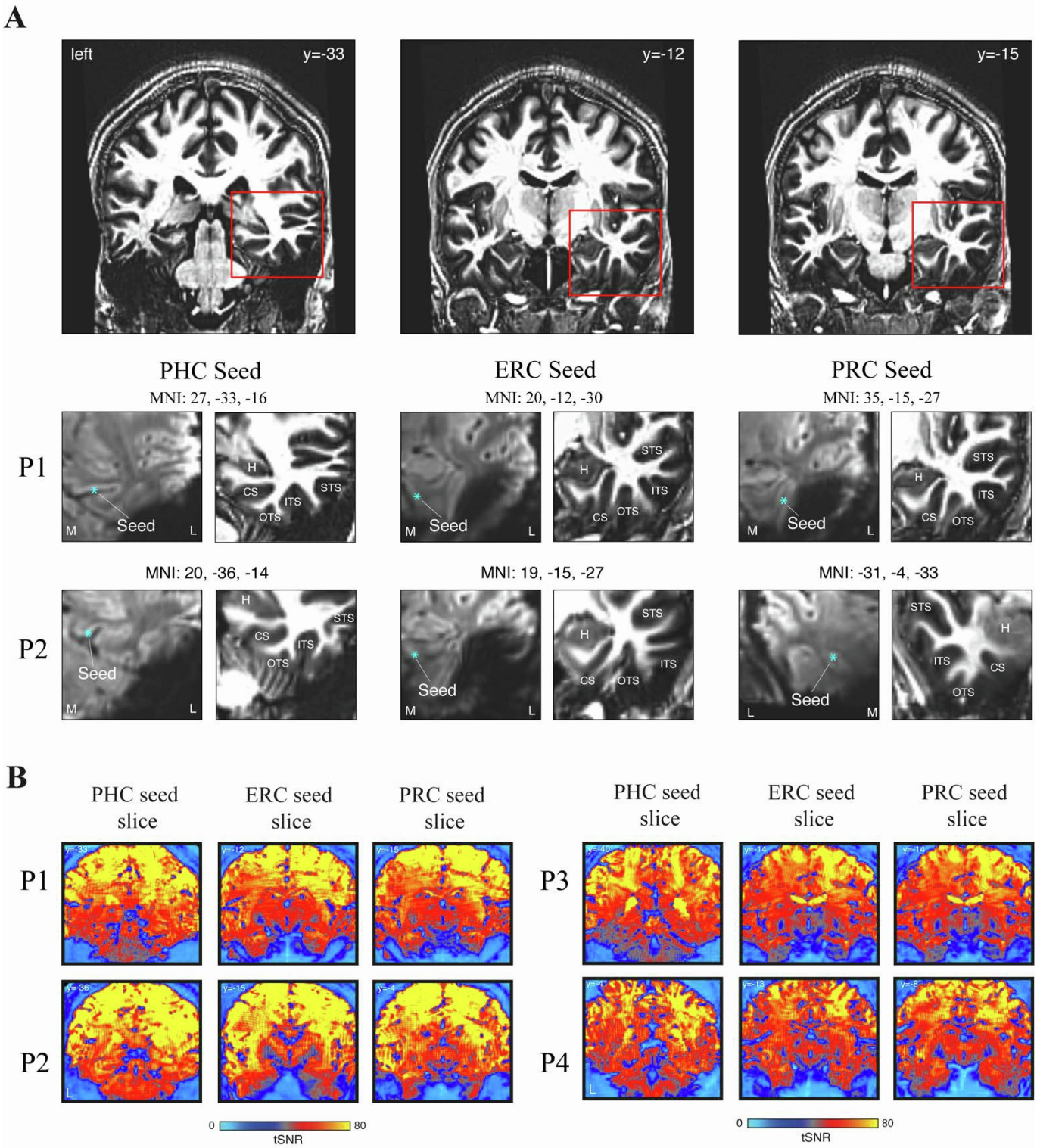
A
left
y=-33
y=-12
y=-15
PHC Seed
MNI: 27, -33, -16
ERC Seed
MNI: 20, -12, -30
PRC Seed
MNI: 35, -15, -27
P1
MNI: 20, -36, -14
MNI: 19, -15, -27
MNI: -31, -4, -33
P2
Seed
M
L
H
CS
STS
ITS
OTS
B
PHC seed slice
ERC seed slice
PRC seed slice
P1
P2
P3
P4
0
80
tSNR

Figure S2. Seed regions in the MTL. Related to Figures 1-2 in the main text and Figure S1.

(A) Coronal slices of the medial temporal lobe from participants 1 and 2 (P1, P2) showing the seed regions in the parahippocampal (area TH, PHC), entorhinal (ERC) and perirhinal (PRC) cortices on T1 and mean BOLD data respectively (seeds are marked with cyan asterisks). Note excellent coverage of the perirhinal and entorhinal cortices. See Figure 2 for the same data from participants 3 and 4. M – medial; L – lateral.

(B) TSNR of the 7T fMRI data. Coronal images presenting tSNR at slices used as seeds in the parahippocampal, entorhinal and perirhinal cortices. Left on the image (L) refers to left hemisphere.

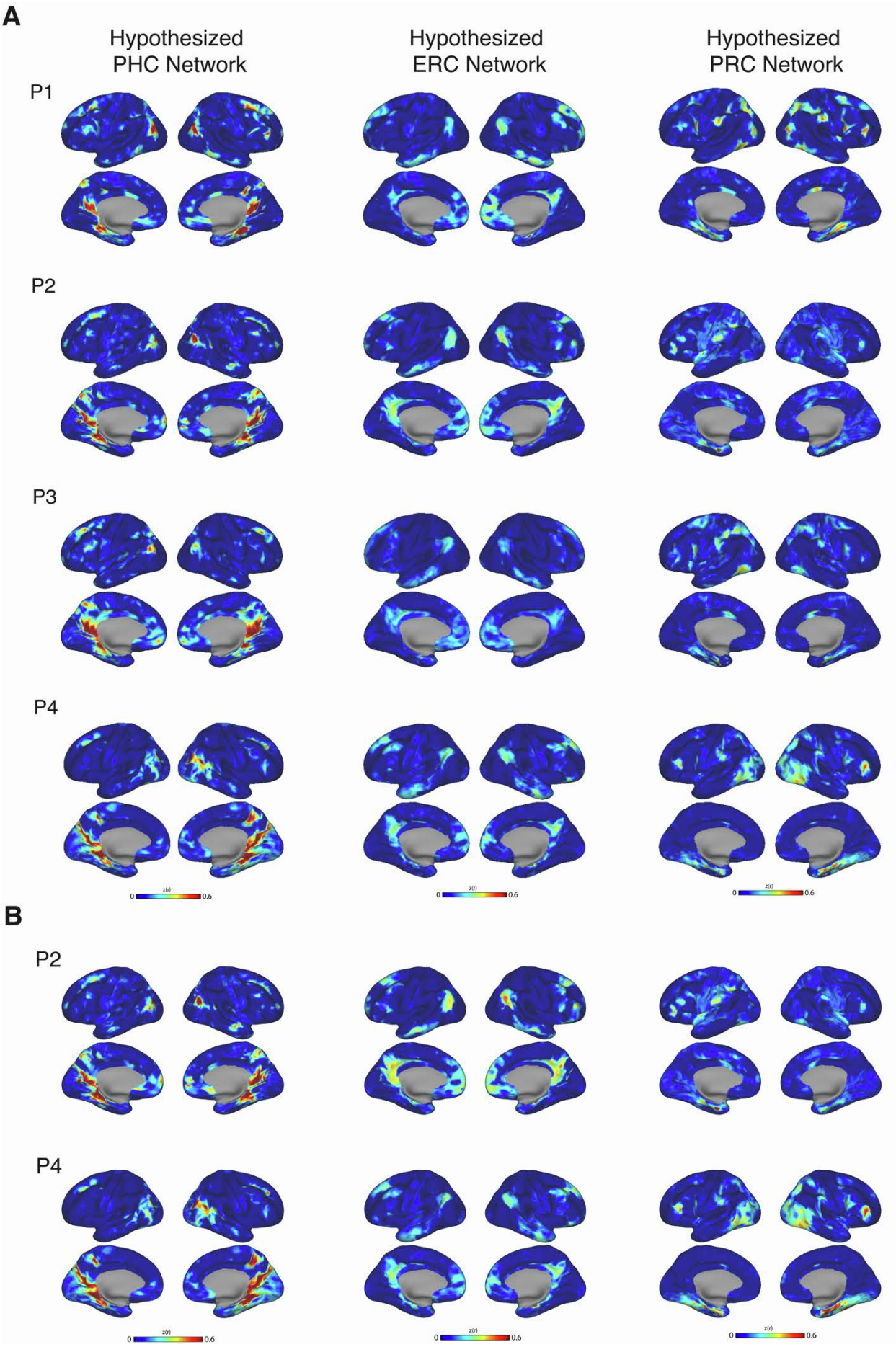
A
Hypothesized PHC Network
Hypothesized ERC Network
Hypothesized PRC Network
P1
P2
P3
P4
0
z(r)
0.6
B
P2
P4

Figure S3. Subregions of the MTL are associated with distinct cortical networks. Related to Figure 3 in the main text.

(A) Bilateral surface-projected and unthresholded functional connectivity maps produced for each MTL seed region in each participant (P1 – P4) using the discovery datasets.

(B) Bilateral surface-projected and unthresholded functional connectivity maps produced for each MTL seed region in P2 and P4 using data that were smoothed with a 4 mm FWHM kernel.

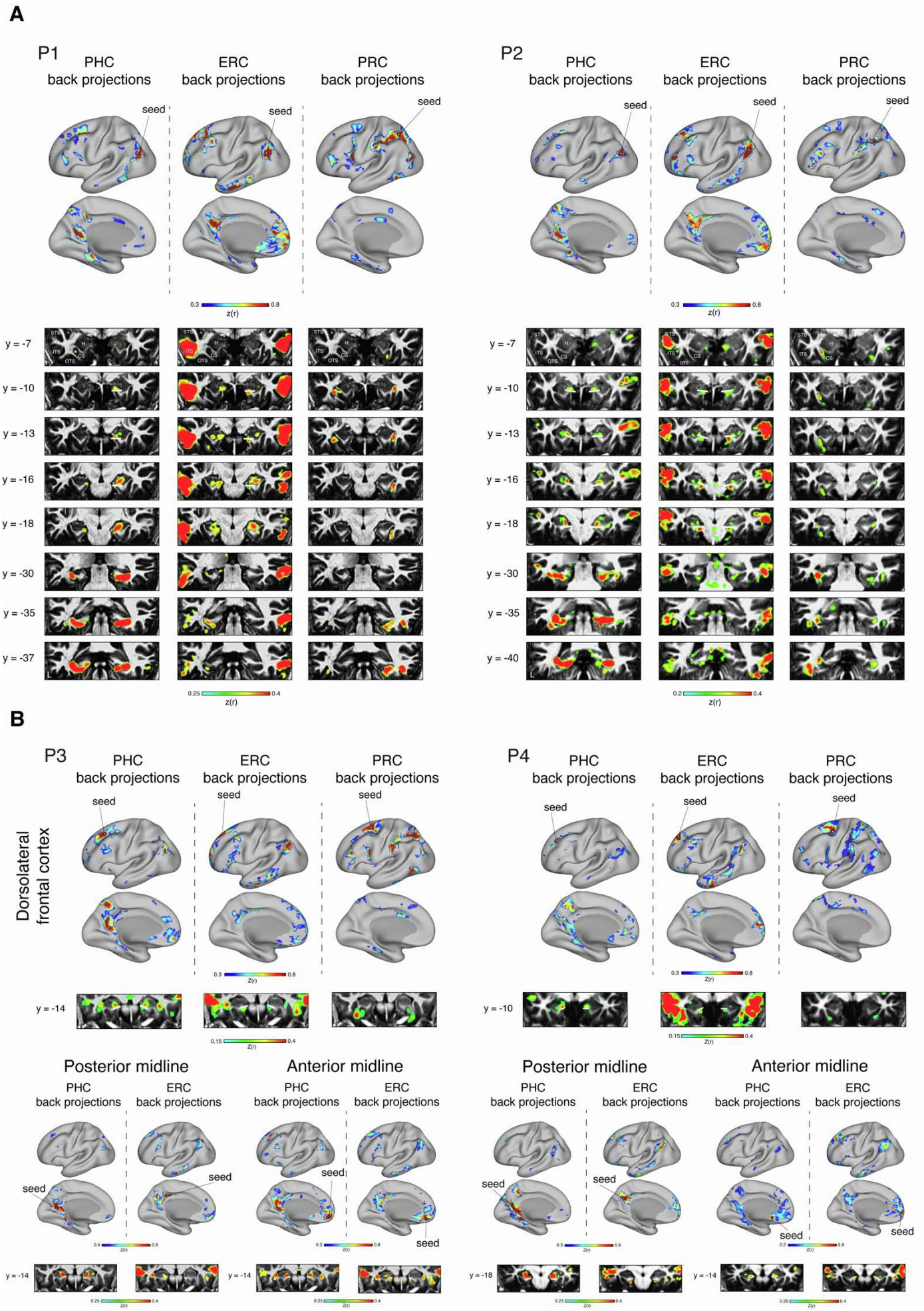
A
P1
PHC
back projections
ERC
back projections
PRC
back projections
seed
z(r)
y = -7
y = -10
y = -13
y = -16
y = -18
y = -30
y = -35
y = -37
P2
y = -40
B
P3
P4
Dorsolateral
frontal cortex
y = -14
Posterior midline
Anterior midline
y = -18

Figure S4. Back projections from parietal cortex seeds – Participant 1 and Participant 2. Back projections from seeds in dorsolateral frontal cortex, anterior midline and posterior midline – Participant 3 and Participant 4. Related to Figure 5 in the main text.

(A) *Top* - surface-projected functional connectivity maps produced for each parietal lobe seed in P1 and P2 using the validation dataset. *Bottom* – coronal slices through the MTL showing correlations with the parietal lobe seeds. Note the bilaterally distinct connectivity patterns in the MTL for different parietal lobe seeds. Also note the distinct connectivity patterns in the anterior MTL associated with caudal and rostral portions of the inferior parietal lobule (separated by the white line). See Figure 5 in the man text for the same data from participants 3 and 4. Left on the image (L) refers to left in the brain.

(B) Similar to Figure 5 in the main text and Figure S4A. Note the distinct connectivity patterns in the anterior MTL separated by the white line. Also note more blurred network distinction using anterior midline seeds in P4, most likely due to lower signal quality in ventral medial prefrontal cortex.

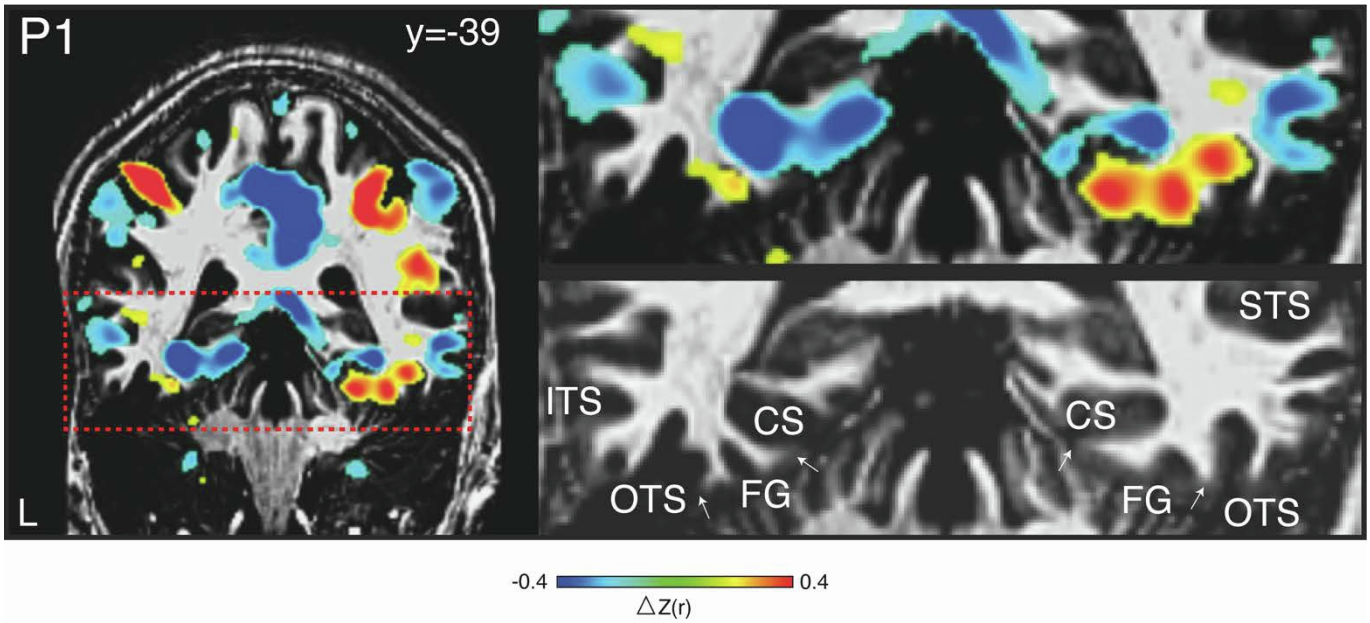

Figure S5. Different subregions of the parahippocampal cortex are differentially associated with retrosplenial cortex and the area anterior to MT+. Related to Figure 6B in the main text. Using all available BOLD data, this additional exploratory analysis shows difference in functional connectivity maps between the retrosplenial and the area anterior to MT+ seeds in P1. Unlike P3 and P4 (Figure 6B), P1 shows more laterally located preferred connectivity with the area anterior to MT+, in accordance with the parahippocampal areas TH/TF definition proposed by von Economo and Koskinas in 1925. The map was thresholded to best capture the differences between connectivity patterns of the suspected parahippocampal areas TH/TF. Left on the image (L) refers to left hemisphere.

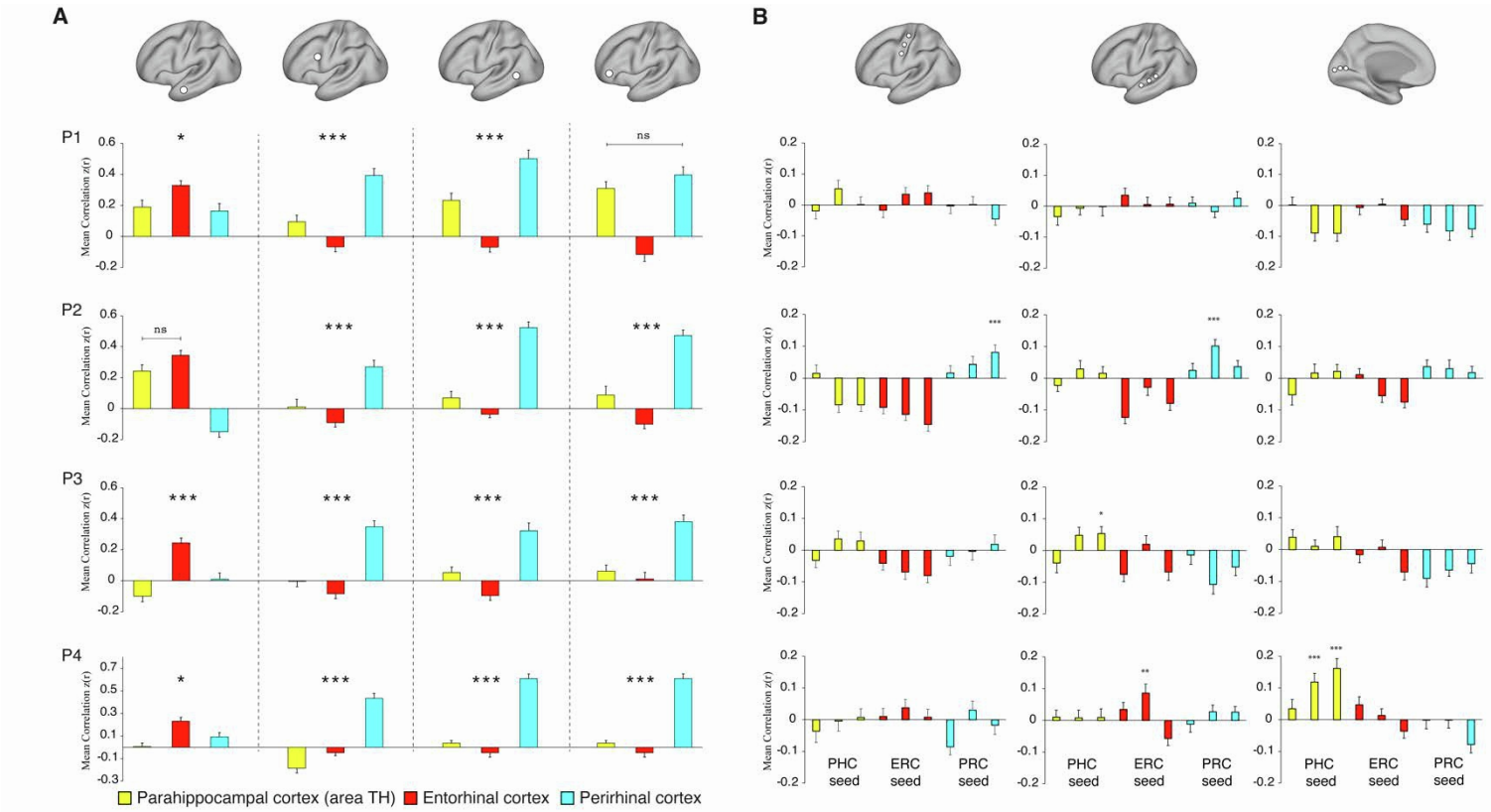

Figure S6. Subregions of the MTL are associated with distinct cortical regions across the cortex and association of subregions of the MTL with sensory systems. Related to Figure 4 in the main text and Figure S3.

(A) In addition to testing the cortical dissociation regions reported in Figure 4 in the main text, we also tested cortical regions that showed connectivity only with the perirhinal cortex - ventral premotor cortex, area anterior to MT+ and anterior lateral frontal cortex. These regions were identified following inspection of the connectivity maps produced during the discovery analysis. Note that since we did not have "competing" MTL seeds that showed anatomically close connectivity patterns in the same cortical region, we performed this comparison *between* different seeds (which we believe is suboptimal, since different seeds can have different connectivity values due to differences in data quality). All hypothesized regions associated with the perirhinal network showed preferred back projection connectivity with the perirhinal cortex, except for the rostral interior frontal gyrus in P1 (all other $p<0.001$).

Moreover, we tested the connectivity of the lateral surface of the temporal lobe (left-most column). In all our participants we observed widespread correlations between the entorhinal cortex and the lateral surface of the temporal lobe, but two participants showed correlations between this brain region and the parahippocampal cortex. Our analysis suggests that the connectivity of the lateral surface of the temporal lobe with the parahippocampal network is variable across individuals.

(B) To examine how the MTL seeds are associated with the somatomotor, auditory and visual systems, in each participant we put three seeds along the central sulcus (somatomotor system), superior temporal gyrus (auditory system), and calcarine sulcus (visual system), anatomically defined. The correlation values between the sensory and MTL seeds were small with only six correlations that were significantly greater than zero, and only one seed showed a correlation value that was greater than noise correlation level ($z(r) = 0.15$). It is important to mention that in this analysis we examined only the association between early sensory systems and the MTL using anatomically defined areas. To provide a full characterization of the interactions between different sensory modalities and the human MTL, future studies combining both task-based and connectivity-based approaches are needed. Bars are mean correlations across all available validation dataset runs ± SEM; * $p < 0.05$; ** $p < 0.01$; *** $p < 0.001$.

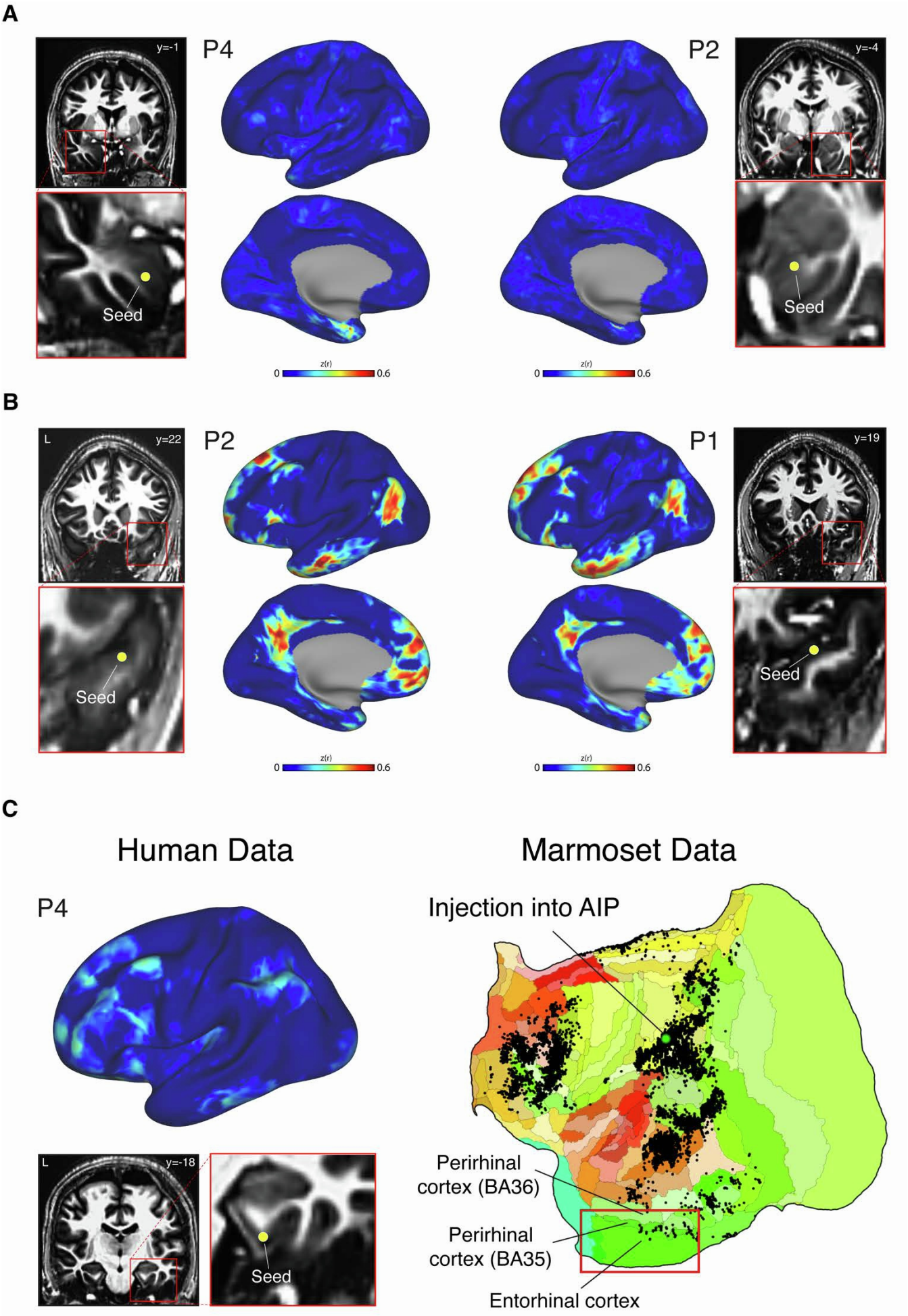
A
y=-1
P4
P2
y=-4
Seed
Seed
z(r)
0
0.6
z(r)
0
0.6
B
L
y=22
P2
P1
y=19
Seed
Seed
z(r)
0
0.6
z(r)
0
0.6
C
Human Data
Marmoset Data
P4
Injection into AIP
L
y=-18
Seed
Perirhinal
cortex (BA36)
Perirhinal
cortex (BA35)
Entorhinal cortex

Figure S7. Connectivity patterns of the anterior entorhinal cortex and temporal pole, and a candidate network associated with the boundary between the entorhinal and perirhinal cortex in P4. Related to Figure 3 in the main text.

(A) In our attempts to localize the human homologue of the rodent lateral entorhinal cortex, we put seeds in the most anterior part of the suspected entorhinal cortex. As can be seen from the cortical projections of the resulting connectivity patterns, correlations coefficients mostly represented spurious/noise correlations that we could not biologically interpret.

(B) Seeds placed directly in the temporal pole resulted in connectivity patterns that closely resembled the entorhinal cortex network. Since the observed connectivity patterns are not compliant with the reported anatomical connectivity of the monkey area 36d (temporal pole), we do not discuss this finding any further.

(C) *Left* - Seeds placed in the very ventral part of the suspected entorhinal cortex, just prior to the medial wall of the collateral sulcus, were associated with a candidate distributed network that bears some resemblance to the frontoparietal control network. *Right* – tracing data with an injection in the anterior intraparietal area (AIP) displaying a proposed homologue of the human frontoparietal control network in the marmoset. Note the remarkable parallel between the human MTL seed location and the labelled cells in the marmoset entorhinal and perirhinal cortices (red box). Even though the connectivity pattern observed in P4 is compliant with primate anatomy, no other participant in our study provided clear evidence for this association and therefore, we did not explore it any further in this study. Left on the image (L) refers to left hemisphere.

A

Perirhinal network	aMT+	SPL	FEF	PrC_v	PFC_{la}	Insula	$Cing_m$
	7/8	7/8	7/8	6/8	8/8	5/8	8/8
Entorhinal network	IPL_r	$Temp_l$	PFC_{dp}	PFC_{lp}	PCC	PFC_m	OFC
	8/8	8/8	8/8	8/8	8/8	8/8	4/8
Parahippocampal network	IPL_c	$Temp_l$	PFC_{dp}	PFC_{lp}	PFC_{la}	RSC	PFC_m
	8/8	3/8	8/8	5/8	3/8	8/8	8/8

B

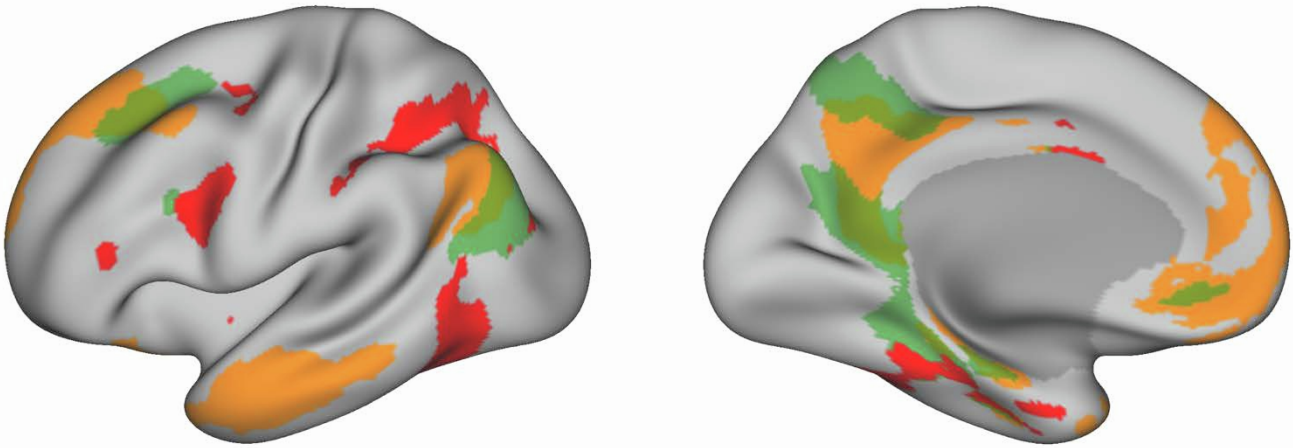

Putative Perirhinal Cortex

Putative Entorhinal Cortex Putative Parahippocampal cortex

Figure S8. Spatial consistency of the cortical areas associated with subregions of the MTL and replication using UK-Biobank data. Related to Figure 8 in the main text.

(A) Based on visual inspection of the unthresholded connectivity maps displayed on Figure S3, we summarized the general consistency of the cortical areas that were associated with parahippocampal area TH, the entorhinal and perirhinal cortices. Numbers represent consistency of major connectivity patterns for each MTL subregions across 8 hemispheres (4 participants with 2 hemispheres each). Note that most of the presented cortical areas were statistically dissociated (see Figure 4 and Figure S6A). aMT+ - area anterior to MT+; SPL – superior parietal lobe; FEF – frontal eye field (or around it); PrC_v – precentral gyrus, ventral; PFC_{la} – prefrontal cortex, lateral anterior; $Cing_m$ – medial segment of the cingulate cortex; IPL_r – inferior parietal lobule, rostral; IPL_c - inferior parietal lobule, caudal; $Temp_l$ – temporal lobe, lateral surface; PCC – posterior cingulate cortex; PFCdp – prefrontal cortex dorsal posterior; PFC_m – prefrontal cortex, medial; OFC – orbitofrontal cortex PFC_{lp} – prefrontal cortex lateral posterior; RSC – retrosplenial cortex.

(B) Seeds put into the putative entorhinal, perirhinal and parahippocampal cortices on the population-level data revealed distributed cortical networks that are similar to the networks we observed on the individual-subject level. Note that the interpretation of these population-level connectivity data is straightforward given our individual-level findings.

	Posterior Entorhinal Cortex	Perirhinal Cortex
P1		
Perirhinal Cortex	0.07	
Parahippocampal Area TH	0.06	0.3
P2		
Perirhinal Cortex	0.01	
Parahippocampal Area TH	0.11	0.12
P3		
Perirhinal Cortex	0.1	
Parahippocampal Area TH	0.03	0.04
P4		
Perirhinal Cortex	-0.06	
Parahippocampal Area TH	0.1	0.08

Table S1. Connectivity between the MTL subregions. Related to Figure 3 in the main text. In each participant, we calculated the mean Fisher z-transformed Pearson correlation coefficients between the entorhinal, perirhinal and parahippocampal seeds. As can be seen from the table, almost all connectivity values were low and did not pass the noise correlation level (z(r) = 0.15). Nevertheless, these findings potentially can be explained by recent anatomical tract-tracing data in the rodent and by re-evaluation of existing anatomical data in the primate (see STAR Methods for more details and discussion).